Cell and Tissue Research
https://doi.org/10.1007/s00441-023-03810-5

REGULAR ARTICLE

Regeneration in calcareous sponge relies on 'purse-string' mechanism and the rearrangements of actin cytoskeleton

Kseniia V. Skorentseva[1] · Fyodor V. Bolshakov[2] · Alina A. Saidova[3,4] · Andrey I. Lavrov[2]

Received: 28 November 2022 / Accepted: 5 July 2023

Abstract

The crucial step in any regeneration process is epithelization, i.e. the restoration of an epithelium structural and functional integrity. Epithelization requires cytoskeletal rearrangements, primarily of actin filaments and microtubules. Sponges (phylum Porifera) are early branching metazoans with pronounced regenerative abilities. Calcareous sponges have a unique step during regeneration: the formation of a temporary structure, called regenerative membrane which initially covers a wound. It forms due to the morphallactic rearrangements of exopinaco- and choanoderm epithelial-like layers. The current study quantitatively evaluates morphological changes and characterises underlying actin cytoskeleton rearrangements during regenerative membrane formation in asconoid calcareous sponge *Leucosolenia variabilis* through a combination of time-lapse imaging, immunocytochemistry, and confocal laser scanning microscopy. Regenerative membrane formation has non-linear stochastic dynamics with numerous fluctuations. The pinacocytes at the leading edge of regenerative membrane form a contractile actomyosin cable. Regenerative membrane formation either depends on its contraction or being coordinated through it. The cell morphology changes significantly during regenerative membrane formation. Exopinacocytes flatten, their area increases, while circularity decreases. Choanocytes transdifferentiate into endopinacocytes, losing microvillar collar and flagellum. Their area increases and circularity decreases. Subsequent redifferentiation of endopinacocytes into choanocytes is accompanied by inverse changes in cell morphology. All transformations rely on actin filament rearrangements similar to those characteristic of bilaterian animals. Altogether, we provide here a qualitative and quantitative description of cell transformations during reparative epithelial morphogenesis in a calcareous sponge.

Keywords Actin filaments · Actomyosin cable · Epithelisation · Morphogenesis · Porifera

Introduction

Cell motility plays key role in embryogenesis, wound healing, and immune response. Changes in cell morphology and migration potential occur due to cytoskeletal rearrangements, in particular, due to coordinated functioning of an actomyosin complex and the presence of cell adhesions anchoring the cell to the substrate or binding it to the other cells (Babbin et al. 2009; Letort et al. 2015).

Healing epithelial wounds is of crucial importance to restoring the internal environment of any animal. It was considered for a long time that embryonic wounds are healed by a special actin 'purse-string' mechanism (Martin and Lewis 1992; Brock et al. 1996): cells at the leading edge of the wound form a continuous actomyosin ring and its contraction pulls wound edges together. On the contrary, epithelial wounds in adult organisms were considered to be healed by extension of lamellipodia from cells at the leading edge followed by their collective migration into the wound (Pang et al. 1978; Zahm et al. 1991; Kretschmer et al. 2017). During the process, epithelial cells lose their apical/basolateral polarity and flatten (Bement et al. 1993). However, the recent data brought the problem to a

✉ Kseniia V. Skorentseva
skorentseva.ksenya.2016@post.bio.msu.ru

1 Laboratory of Morphogenesis Evolution, Koltzov Institute of Developmental Biology of Russian Academy of Sciences, 26 Vavilov Street, Moscow 119334, Russia

2 Pertsov White Sea Biological Station, Faculty of Biology, Lomonosov Moscow State University, Leninskiye Gory, 1 Build. 12, Moscow 119234, Russia

3 Department of Cell Biology and Histology, Faculty of Biology, Lomonosov Moscow State University, Leninskiye Gory, 1 Build. 12, Moscow 119234, Russia

4 Engelhardt Institute of Molecular Biology, Russian Academy of Sciences, 32 Vavilov Street, Moscow 119991, Russia

Published online: 19 July 2023

new level of complexity. To date, two major mechanisms, purse-string and collective cell migration, are considered to interact with each other through the crosstalk of signalling pathways (Anon et al. 2012; Brugués et al. 2014; Kuipers et al. 2014), in particular through the functioning of the Rho family of GTPases (Nobes and Hall 1995; Fenteany et al. 2000; Tamada et al. 2007).

Sponges (phylum Porifera) are one of the most basal metazoan groups, which had long independent evolution (Simion et al. 2017). Sponges have a distinctive body plan and possess unique regenerative capacities ranging from wound healing to complete restoration of functional organism from dissociated cells (Lavrov and Kosevich 2014; Ereskovsky et al. 2021). The mechanisms of regeneration vary significantly among sponge clades. The regeneration in Demospongiae relies on various transformations of individual cells: dedifferentiation, transdifferentiation, epithelial-mesenchymal transition (EMT), and mesenchymal-epithelial transition (MET) (Alexander et al. 2015; Borisenko et al. 2015; Ereskovsky et al. 2020). In contrast, regeneration in Calcarea is based on coordinated interaction of the epithelial-like cell layers with no contribution of proliferation to wound healing process (Lavrov et al. 2018; Caglar et al. 2021). This process requires cell transdifferentiation and epithelial transformations followed by loss of characteristic cell features (Lavrov et al. 2018; Ereskovsky and Lavrov 2021).

Essential studies on calcareous sponge regeneration were carried out mainly using light and electron microscopy (Korotkova 1961, 1963; Padua and Klautau 2016; Ereskovsky et al. 2017; Lavrov et al. 2018). At the site of the injury, cells of the body wall form a two-layered semi-transparent membrane, regenerative membrane (RM). The process has two phases: the membrane formation itself and its transformation into the normal body wall, i.e. choanoderm formation on its inner side, porocytes development, and spiculogenesis. Regeneration proceeds due to the rearrangements and migration of the epithelial-like cell layers (pinaco- and choanoderm) without loss of cell–cell adhesions or proliferation (Korotkova 1961, 1963; Lavrov et al. 2018; Caglar et al. 2021).

Currently, data on the structure of actin filaments in sponge cells are fragmentary and obtained primarily for freshwater sponges (Pavans de Ceccatty 1981, 1986; Wachtmann et al. 1990; Gaino and Magnino 1999), and the most detailed studies describe the role of the actin cytoskeleton in the formation of cell adhesions (Miller et al. 2018; Mitchell and Nichols 2019; Green et al. 2020). The role of cytoskeletal rearrangements in morphogenetic processes during embryogenesis and regeneration in sponges remains poorly elucidated.

In the current study, we examined the general dynamics and rearrangements of actin filaments in main cell types during body wall regeneration in asconoid calcareous sponge *Leucosolenia variabilis* using immunocytochemistry, confocal laser scanning microscopy, and live time-lapse imaging. Our study reveals cytoskeleton rearrangements underlying transformations of epithelial-like cell layers (exopinacoderm and choanoderm) and formation of contractile actomyosin cable on the leading edge of the wound. We show significant changes in cell morphology during this epithelial morphogenesis. We also studied the morphology and dynamic parameters of the individual mesohyl cells in the RM, thus providing new data on epithelial morphogenesis as the main force of regeneration in calcareous sponges.

Materials and methods

Sampling and surgical operation

Specimens of *Leucosolenia variabilis* Haeckel, 1870 (Calcarea, Leucosolenida) were collected during summer seasons 2019–2022 in Kandalaksha Bay, the White Sea, in the vicinity of the Pertsov White Sea Biological Station of Lomonosov Moscow State University (66°34′N, 33°08′E). The specimens were collected in the upper subtidal zone (0–2 m) during low tides and stored in the flow-through aquarium for no longer than 10 days.

As a regeneration model in this study, we used ring-shaped body fragments from oscular tubes. The operation procedures were performed in 0.22-µm-filtered seawater (FSW). Sponges were rinsed from debris, and oscular tubes were cut off and collected. Each oscular tube was transversely cut into ring-shaped body fragments 1–3 mm width (the osculum rims were excluded). All surgical operations were performed manually under a stereomicroscope using Castroviejo scissors. Body fragments were maintained in Petri dishes with 5 ml FSW at the physiological temperature 8–12 °C (see Online Resource 1). Half of the FSW medium was changed every 12 h. Regular observations were made to prevent contamination and assess the stage of regeneration.

Time-lapse imaging and functional experiments

To visualise regenerative membrane growth and track individual mesohyl cells under normal conditions as well as under inhibitory treatment, time-lapse imaging was performed using a Nikon TI-S inverted microscope (Nikon Instruments Inc., USA) equipped with a ToupCam U3CMOS05100KPA digital camera (Touptek Photonics, China) (application ToupView v. 3.7) and a cooling microscopic stage.

To record normal regeneration process, ring-like body fragments were kept in glass bottom Petri dishes with 5 ml FSW at temperatures of 8–12 °C. To demonstrate the contractile function of the actomyosin cable, fragments with incomplete RM were maintained in 5-ml glass bottom Petri dishes with 50 µM blebbistatin (AdooQ BioScience A13647,

USA) for 300 min. The membrane growth was filmed with an objective 20× LWD Achromat 0.40 Ph1 ADL WD 3.1 ∞/1.2 OFN25 (Nikon Instruments Inc.) with an additional lens of 0.5× with 30-s intervals between frames. For cell tracking, an objective 40× ELWD S Plan Fluor 0.60 Ph2 ADM WD 3.6–2.8 ∞/0–2 OFN22 (Nikon Instruments Inc.) with an additional lens 0.5× was used; interval between frames was 15 s (Lavrov and Ereskovsky 2022).

To perform cell tracking, the MTrackJ plugin in ImageJ v.1.53c (National Institute of Health, Bethesda) was used. We calculated total track distance, total displacement (the length of line connecting first and last track point), the average cell velocity (dividing the total track distance by the acquisition time), and migration efficiency (dividing the total displacement by the track length). The measurements were performed at two stages of regeneration: during the active membrane growth (12–24 hours past operation, or hpo) and in full membrane during choanocyte redifferentiation (24–48 hpo).

The following programs were used to create time-lapse films: ImageJ v.1.53c, Adobe Photoshop Lightroom Classic V.10.3 (Adobe Inc., USA), VirtualDub (https://www.virtualdub.org), Adobe Premier Pro V.22.1.2 (Adobe Inc., USA), and Handbrake (https://github.com/HandBrake/HandBrake).

Immunostaining

Four fixation methods were used: 4% paraformaldehyde (Carl Roth 0335.2) in phosphate-buffered saline (PBS, Eco-Servis B-60201); 4% paraformaldehyde (Carl Roth 0335.2) in FSW; 2.5% glutaraldehyde (EMS 16220) in PBS at 4°C for at least 4 h; ice-cold methanol (Merck 106.008) for 1 h followed by 4% PFA in PBS at 4 °C overnight. All fixation methods provided comparable results.

After fixation, the samples were rinsed with PBS three times. To prevent autofluorescence of glutaraldehyde, samples were incubated in three changes of 1–3% sodium borohydride ($NaBH_4$, Panreac 163.314) for an hour. The samples were then blocked with a solution of 1% bovine serum albumin (BSA, MP Biomedicals 0216006980), 0.1% cold-water fish skin gelatine (Sigma-Aldrich G7041), 0.5% Triton X-100 (Sigma-Aldrich T8787), and 0.05% Tween-20 (Sigma-Aldrich P1379) in PBS and incubated overnight at 4°C in primary antibodies: anti-human actin-β primary monoclonal antibody produced in mouse (1:100; Bio-Rad Laboratories Inc. MCA57766A) and non-muscle myosin II produced in rabbit (1:100, Sigma-Aldrich M8064). In some samples, Phalloidin FITC (1:200, Sigma-Aldrich P5282) was used instead of primary antibodies to reveal actin filaments, since staining patterns appeared equal. After incubation with antibodies, the samples were rinsed three times in the blocking solution and incubated for 4 h in goat polyclonal secondary antibody to mouse IgG conjugated with AlexaFluor 555 (1:100, Invitrogen A31570) and donkey polyclonal secondary antibody to rabbit IgG conjugated with AlexaFluor 647 (1:100, Invitrogen A10040). Finally, the samples were rinsed three times in PBS and stained with 2 µg/ml 4′,6-diamidino-2-phenylindole (DAPI, Acros 202.710.100) in PBS for 1 h. Rinsed specimens were mounted in 90% glycerol (MP Biomedicals 193,996) with 2.5% 1,4–23 diazabicyclo[2.2.2]octane (DABCO, Sigma-Aldrich D27802) and examined with a CLSM Nikon A1 (Nikon, Shinagawa, Japan) using lasers with 405, 546, and 647 nm wavelength.

Image processing and statistical analysis

The obtained Z stacks (step 200–300 nm) were processed with ImageJ v.1.53c to describe actin structures in different cell types and define morphological parameters of the cells: area, circularity, and aspect ratio. For intact exopinacocytes, the cell body and cytoplasmic plate were analysed separately. Circularity was calculated with the following formula:

$$4\pi \times \left(\frac{cell\ area}{cell\ perimeter^2}\right) \quad (1)$$

A high circularity value (tending to 1.0) indicates fewer cell protrusions (such as filopodia or lamellipodia) and a low value (tending to zero)—the unevenness of the cell edges. The aspect ratio (AR) was calculated using the following formula:

$$\frac{length\ of\ the\ major\ axis\ of\ the\ cell}{lenght\ of\ the\ minor\ axis\ of\ the\ cell} \quad (2)$$

It illustrates how elongated the cell is: the higher values correspond to narrower and longer cells. To obtain these parameters, cell images were outlined using the 'Freehand selection' tool and "ROI manager". The raw data is provided in Online Resources 2 and 3.

The digital photos were processed in ImageJ v.1.53c. Gaussian blur, changing the brightness-contrast parameters and background subtraction were applied to 16-bit images for noise reduction and contrast enhancement. This processing sequence was used both for time-lapse imaging and confocal images.

To compare the morphological parameters of different cell types and the dynamic parameters of mesohyl cells, the following statistical tests were used: the Mann-Whitney *U*-test and Kruskal-Wallis test by ranks followed by post hoc Dunn's multiple comparisons test with Benjamini-Hochberg correction. Firstly, the datasets were tested for normality with the Shapiro-Wilk test and outliers were excluded using the ROUT method ($Q = 5\%$) in Prism 8.0.1 (GraphPad Software, USA). Subsequent comparisons were handled using an

appropriate statistical test (multiple comparisons/not multiple). A test used is indicated in each case individually. These statistical procedures and data visualisation were performed in RStudio version 4.0.3 (RStudio, USA). All the data are expressed as mean ± s.e.m. (standard error of mean). The significance level was 0.05.

Results

Leucosolenia variabilis has an asconoid body plan. Its body wall has a thickness of 20–30 µm and contains three cell layers: the outer exopinacoderm, the inner choanoderm, and intermediate mesohyl, which contains a few migrating cells and the extracellular matrix (Fig. 1a, b).

Actin structures in cells of the intact body wall

Intact exopinacocytes are T-shaped (Fig. 2a, b); their cell body is submerged into the mesohyl matrix and has a few filopodia linking exopinacocytes to each other (Fig. 2b). Each exopinacocyte also has a flat polygonal external part (Fig. 2a), a cytoplasmic plate, which is connected with the cell body (Fig. 2b) through a thin 'neck'. Cytoplasmic plates represent the outer layer of the body wall; thin actin bundles at their periphery delineate cell margins (Fig. 2a).

Porocytes represent a specific cell type penetrating the sponge body wall from the exopinacoderm to choanoderm (Fig. 2c). Porocyte is cylindrical cell with an ostium, pass-through intracellular canal connecting the environment with the inner lumen of the sponge lined by the choanoderm. Actin filaments in porocytes are also represented by cortical actin bundles and numerous filopodia (Fig. 2c).

Choanocytes are tightly packed prismatic cells with an apical ring of actin-cored microvilli (Fig. 3a) located around a flagellum. Most actin structures in choanocytes are also cortical actin bundles (Fig. 3a, b).

Mesohyl cells form a heterogeneous population. They differ in morphology and, most likely, in function. Using immunocytochemistry, we distinguished three cell types—large amoebocytes, sclerocytes, and granular cells (Fig. 4).

Large amoebocytes often have an oval nucleus and lobopodia getting thinner and branching at the end (Fig. 4a). Their typical location is in the mesohyl matrix, right above the choanoderm layer. The staining of these cells appears to be homogeneous probably because of background noise of the cytoplasm. Large amoebocytes differ from other mesohyl cells due to their size (224.8 ± 16.78 µm^2, $n = 19$) and lower circularity value (0.0816 ± 0.0122, $n = 19$) caused by branching extensions. AR value is 1.837 ± 0.09 ($n = 19$) indicating that extensions are widely spread in numerous directions (see Online Resource 4).

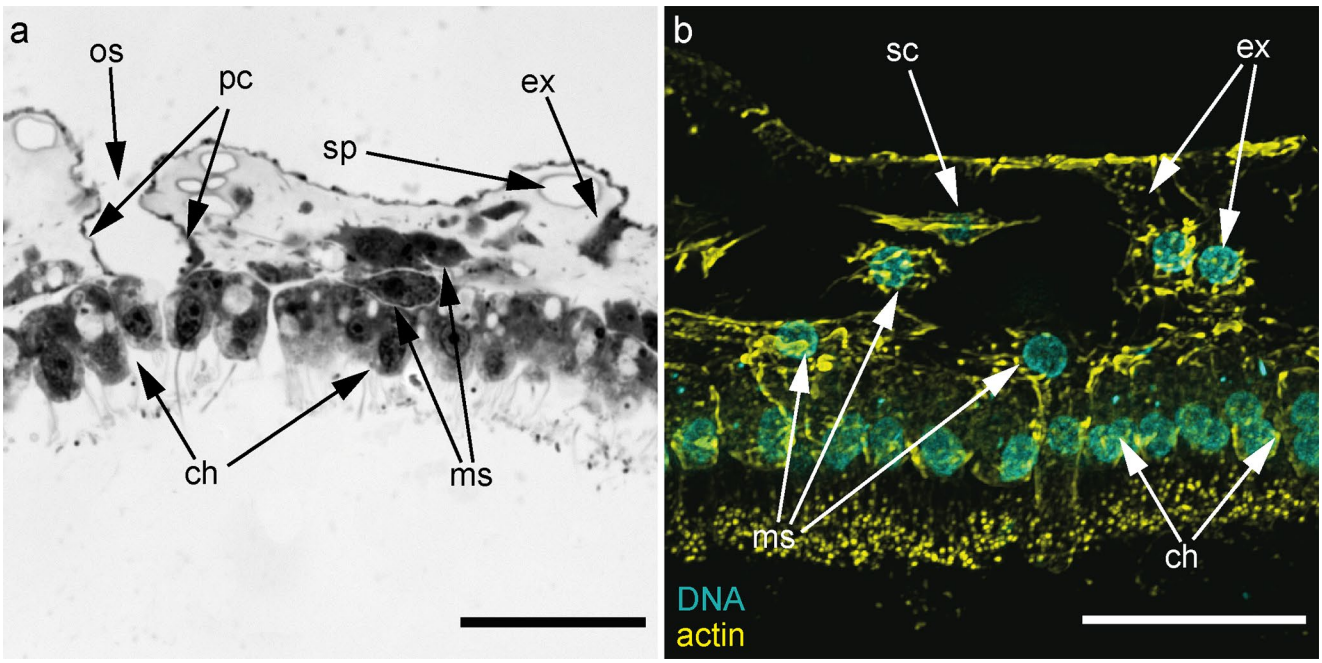

Fig. 1 Histology of *Leucosolenia variabilis* body wall, cross-section through the middle part of the oscular tube. **a** Semi-thin section, light microscopy; **b** CLSM, maximum intensity projection of several focal planes, ice-cold MeOH fixation; cyan – DNA, DAPI; yellow – actin filaments, antibody staining. ch, choanoderm; ex, exopinacocyte; ms, mesohyl cell; os, ostium; pc, porocyte; sc, sclerocyte; sp, spicule. Scale bars: **a**, **b** 20 µm

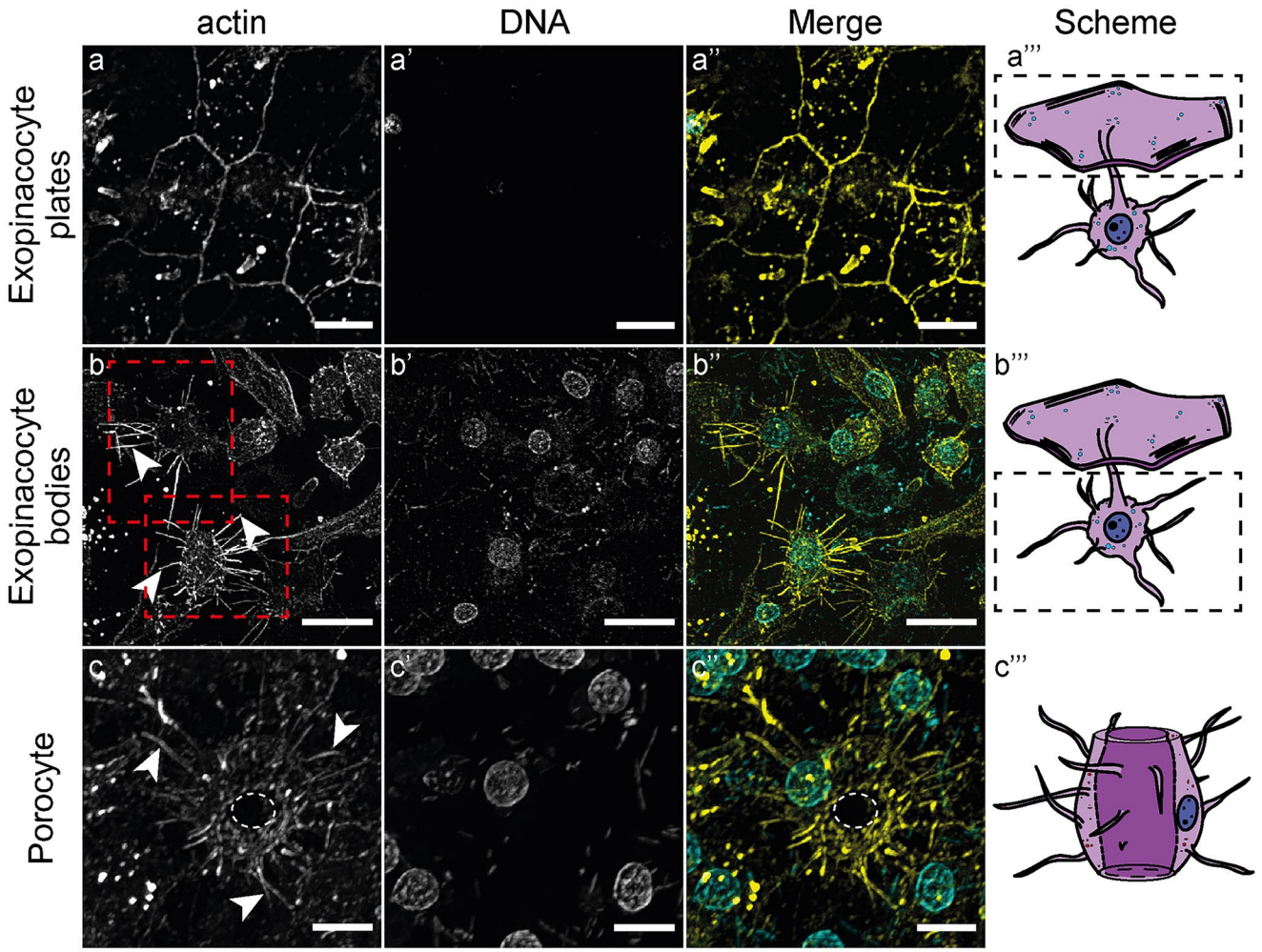

Fig. 2 Actin filaments in the exopinacocytes and porocytes of the intact body wall. **a** Exopinacocyte cytoplasmic plates covering the body surface, 2.5% GlA in PBS fixation; **b** exopinacocyte bodies submerged into mesohyl (red dotted lines), 4% PFA in PBS fixation; **c** porocyte, the white dotted line marks ostia, 4% PFA in PBS fixation; CLSM (maximum intensity projection of several focal planes); cyan – DNA, DAPI; yellow – actin filaments, antibody staining. **a‴**, **b‴**, **c‴** Cell schemes; the black dotted lines outline exopinacocytes parts demonstrated in the row; the white arrowheads mark filopodia. Scale bars: **a**, **b** 10 µm; **c** 5 µm

Sclerocytes have a spindle-like shape, outlined with cortical actin, and often have a few filopodia as well as numerous stress fibers along the major axis (Fig. 4b). Sclerocytes are the only mesohyl cells with distinct non-muscle myosin II pattern along the stress fibers (see Online Resource 5). In intact tissues, these cells have an intermediate area value – 113.9 ± 4.275 µm^2 ($n = 99$) and a low circularity value 0.3048 ± 0.0112 ($n = 99$) (see Online Resource 4). Since the sclerocytes are elongated along with the axis of the spicule they synthesise, the AR value is quite high – 3.019 ± 0.0933 ($n = 99$) (see Online Resource 4).

Granular cells are of intermediate size, with small condensed nucleus and cell edges aligned by cortical actin bundles. These cells have numerous homogeneously stained large granules which alter the morphology of the cell due to dense packing (Fig. 4c). These cells also have an intermediate area values: 84.85 ± 7.751 µm^2 ($n = 6$) and quite high circularity value – 0.6597 ± 0.0501 ($n = 6$) (see Online Resource 4). The AR value (1.555 ± 0.0714, $n = 6$) indicates the slightly elongated form of the cell (see Online Resource 4). Granular cells have season-dependent distribution: these cells are absent in spring and early summer samples, but autumn and winter samples have plenty of them.

General observations on the formation of the regenerative membrane

Ring-shaped body fragments obtained after the operation have two wound areas located in the cut planes. The subsequent regeneration process leads to the formation of new body walls, which close the orifices and are perpendicular to the intact walls of the body fragment (see Online Resource 1).

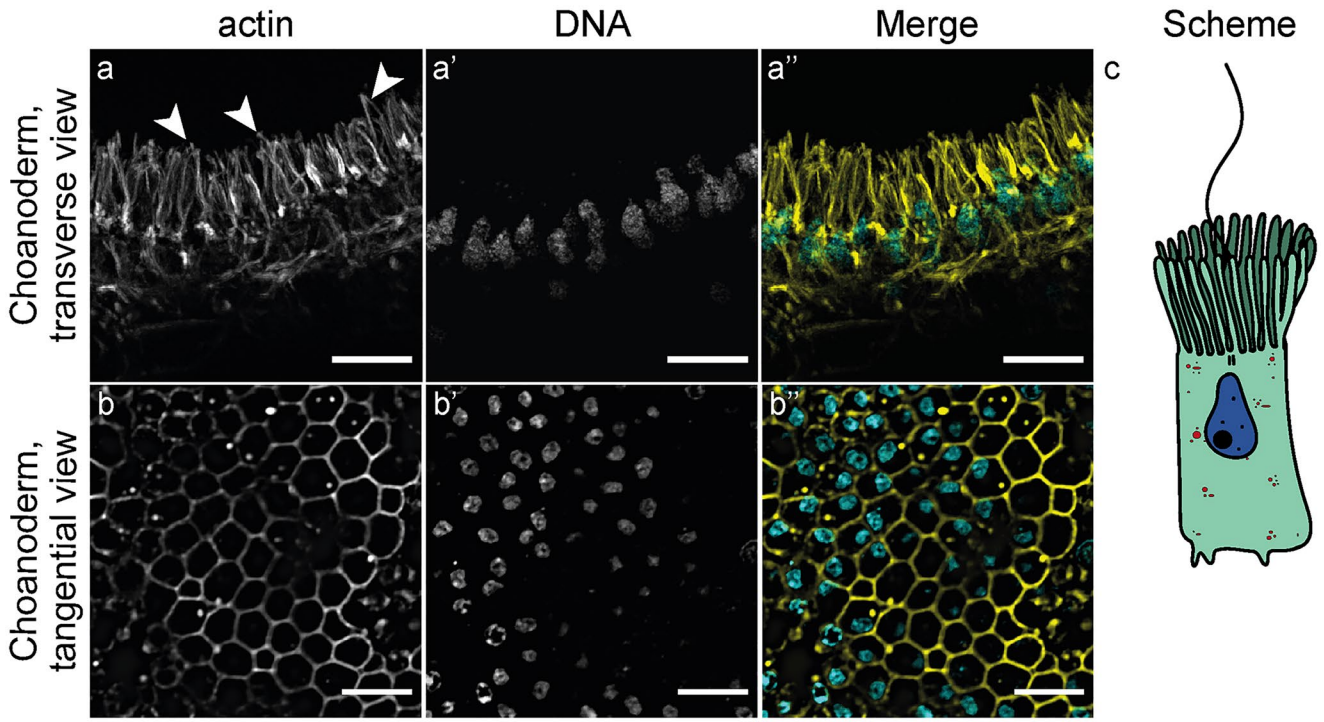

Fig. 3 Actin filaments in the choanocytes of the intact body wall. **a** Choanoderm, transverse view, 4% PFA in FSW fixation; **b** choanoderm, tangential view, 4% PFA in PBS fixation; **c** cell scheme; CLSM (maximum intensity projection of several focal planes); cyan – DNA, DAPI; yellow – actin filaments, phalloidin staining (**a**), antibody staining (**b**). The white arrowheads mark microvilli collars. Scale bars: **a**, **b** 10 µm

The regeneration occurs through the formation of a temporary structure, the regenerative membrane (RM) (see Online Resources 6 and 8). RM appears at ~ 12–24 hpo on the edge of the wound and gradually expands towards its centre, until forming a continuous structure (Fig. 5a–e; Online Resource 6). During growth, RM has a thickness of 10–15 µm and consists of three layers: the external exopinacoderm, the internal endopinacoderm, and very narrow mesohyl in between (Online Resource 6). As shown previously, during RM formation intact T-shaped exopinacocytes flatten into thin polygonal cells, endopinacocytes of RM appear in the wound area through the transdifferentiation of the choanocytes (Lavrov et al. 2018). Mesohyl cells appear in RM through migration from nearby intact tissues. The exo- and endopinacocytes adhesions at the growing rim of RM isolate the mesohyl layer from the external environment.

The complete RM closing the wound orifice usually forms at ~ 48 hpo. However, already at ~ 24–30 hpo, the transformation of RM into the body wall begins. This process includes the restoration of exopinacocytes' T-shape morphology, redifferentiation of endopinacocytes to choanocytes at the internal side of RM, appearance (through transdifferentiation of exopinacocytes) of porocytes penetrating RM, and sclerocytes synthesising new spicules in the RM mesohyl (Lavrov et al. 2018). All these processes begin in the peripheral part of RM and gradually proceed in the centripetal direction. The complete transformation of RM into the body wall ends at 120–144 hpo for body wall cuts (Lavrov et al. 2018), although tracking the process to its end in our model was beyond the scope of the study.

The formation and transformation of the RM rarely appear to be symmetrical: different sides of the RM grow and turn into the body wall at a varying rate. Moreover, time-lapse visualisations clearly show that RM is under significant mechanical tension since sometimes it rips on the leading edge (see Online Resource 7). To describe RM growth dynamics, we analysed it 1–2 h before a complete closure over a wound plane. The RM growth appears to be non-linear process with fluctuations. The obtained data also demonstrate a varying regeneration speed rate between individual specimens (time spent on closing the wound with a perimeter of 4–5 mm varied from 40 to 80 min) (Fig. 5f).

Actin structures in cells of the regenerative membrane

The outer layer of the regenerative membrane is represented by exopinacocytes, while the inner layer depending on the stage of regeneration by endopinacocytes or redifferentiating choanocytes, with a thin layer of mesohyl containing single migrating cells (Fig. 6a).

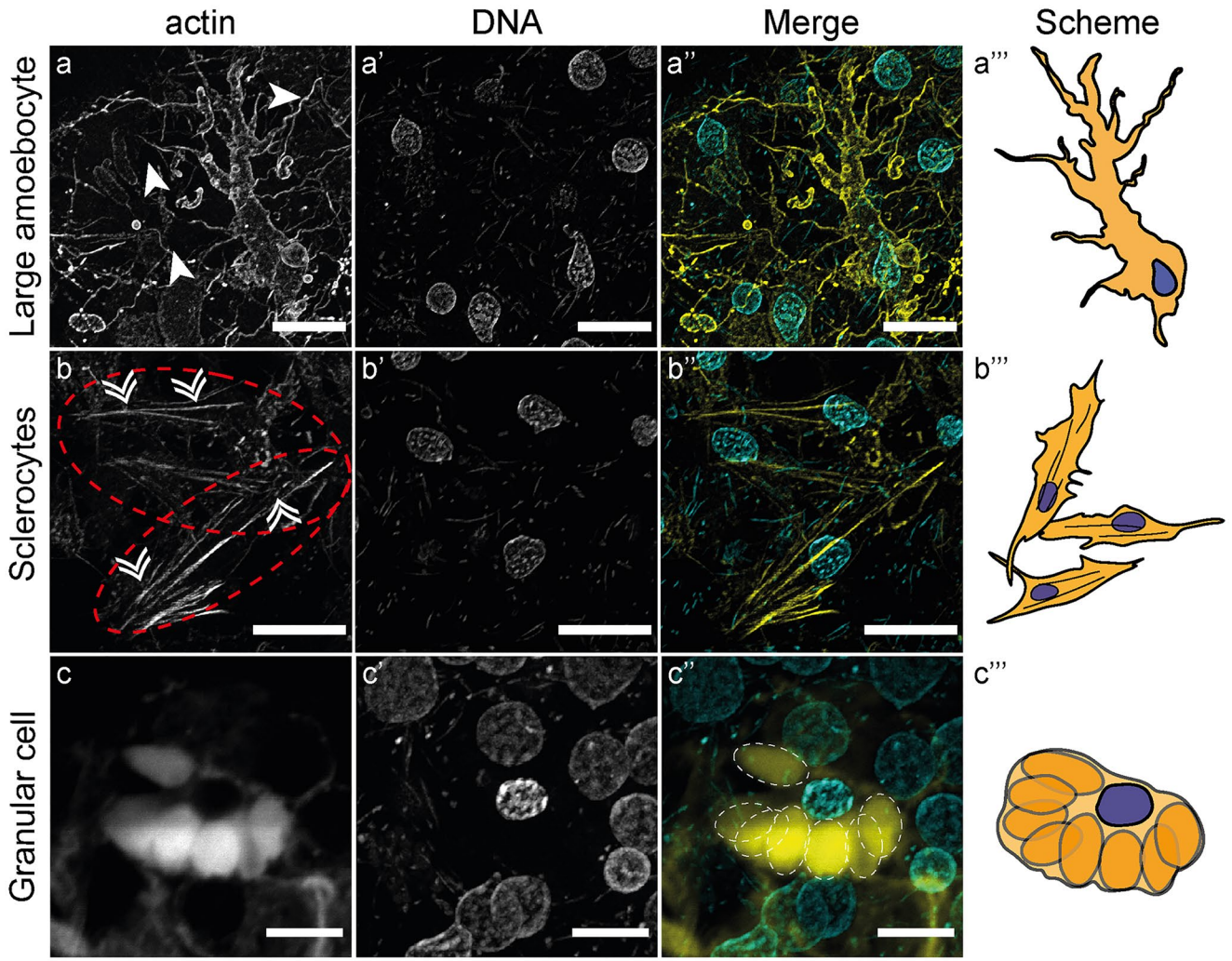

Fig. 4 Actin filaments in the mesohyl cells of the intact body wall. **a** Large amoebocyte, 2.5% GlA in PBS fixation; **b** sclerocytes (red dotted lines), 4% PFA in PBS fixation; **c** granular cell, the white dotted lines outline the edges of autofluorescent granules, 4% PFA in PBS fixation; CLSM (maximum intensity projection of several focal planes); cyan – DNA, DAPI; yellow – actin filaments, antibody staining; **a‴**, **b‴**, **c‴** cell schemes; The white arrowheads mark filopodia, the double arrowheads mark stress fibers. Scale bars: **a**, **b** 10 μm; **c** 5 μm

The actin structures in flat polygonal exopinacocytes of RM are represented by cortical filament bundles (Fig. 6b). The inner layer of the growing RM is represented by flat polygonal endopinacocytes (Fig. 6b) at the early stages of regeneration (0–48 hpo). These cells do not have the collar of microvilli and flagellum. The actin cytoskeleton in these cells consists of cortical bundles of filaments. During the later stage of regeneration (48–96 hpo) when the transformation of the RM into the intact body wall occurs, ball-shaped cells with cortical actin filaments and short microvilli (Fig. 6c) gradually occupy the inner layer of the RM. These are redifferentiating choanocytes. They are packed loosely in comparison with tightly packed prismatic choanocytes of the intact body wall. These choanocytes arise through redifferentiation of the endopinacocytes, occurring from the peripheral sides of RM to its centre.

The mesohyl layer in the RM is quite thin; cells have actin protrusions and migrate intensively through the extracellular matrix. However, we have not seen any stress fibers in them.

The most prominent actin structure of RM is a thick actin cable (Fig. 7a) appearing on its leading edge during the growth stage. The actin cable seems to be formed by pinacocytes (sensu lato). However, the overall thickness of the RM leading edge does not allow to decide if it is formed by exo- or endopinacocytes. The cable runs continuously at the leading edge and is visible until complete sealing of the RM. We have never observed similar actin structures in pinacocytes lying behind the leading edge. Cells at the leading edge of RM also possess small short-living filopodia with a lifetime of ~ 20 time frames (Fig. 7a), which are highly dynamic (Online Resource 6). Non-muscle myosin II colocalises along the cable in

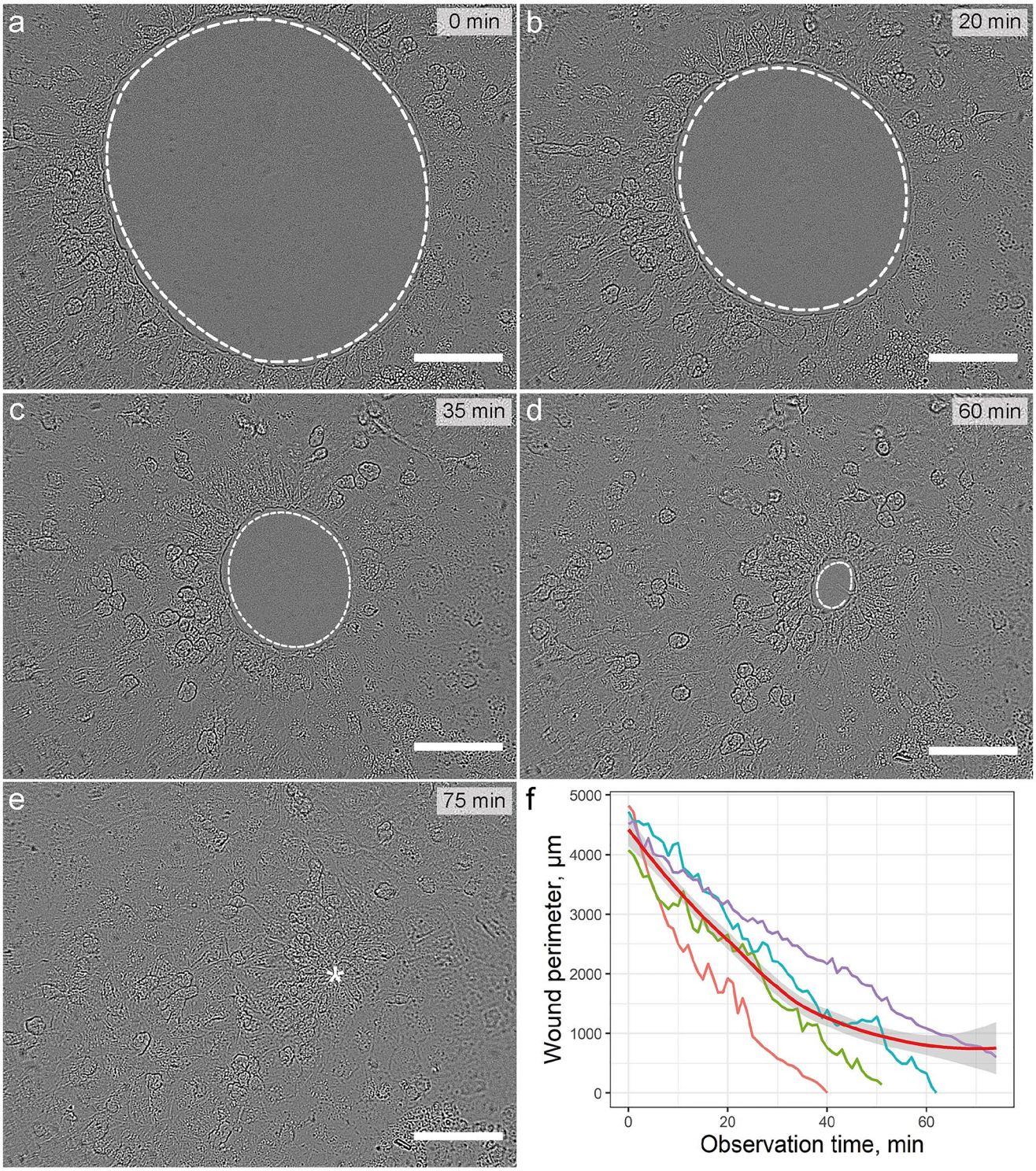

Fig. 5 Dynamics of regenerative membrane (RM) formation prior to full closure (~24 hpo). **a**–**e** RM closure, light microscopy, frames from time-lapse imaging; **f** line plot of closure dynamics ($n=4$); red line is the trend line with a confidence interval (grey background). White dotted lines mark the leading edge of the RM; asterisk mark the RM closure point. Scale bars: **a**–**e** 50 µm

a beaded intermittent pattern (Fig. 7b). This indicates direct binding of myosin with the cable and allows us to define this structure as actomyosin cable with contractile properties (see Online Resource 9). This assumption is confirmed by functional experiments. Addition of specific inhibitor of myosin II, 50 µM of blebbistatin, to

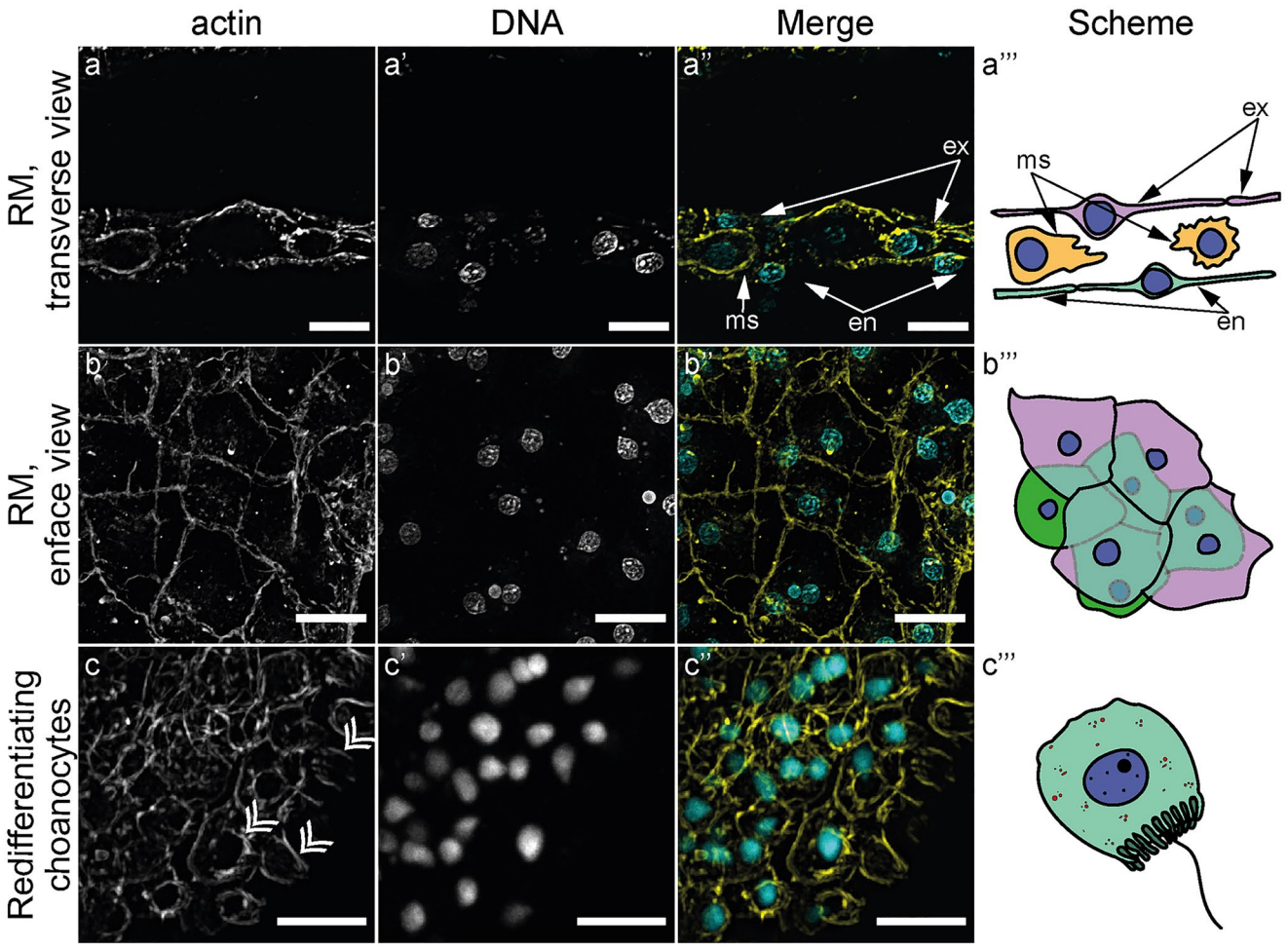

Fig. 6 Actin filaments in the exopinacoderm, endopinacoderm, and choanoderm of the regenerative membrane (RM). **a** RM, optical section demonstrating transverse view, 2.5% GlA in PBS fixation; **b** RM, flat exo- and endopinacocytes, 2.5% GlA in PBS fixation; **c** redifferentiating choanocytes at the periphery of RM, 4% PFA in FSW fixation; CLSM (maximum intensity projection of several focal planes); cyan – DNA, DAPI; yellow – actin filaments, antibody staining (**a** and **b**), phalloidin staining (**c**). **a‴**, **b‴**, **c‴** cells schemes. The double arrowheads mark choanocyte microvilli collar. en, endopinacocytes; ex, exopinacocyte; ms, mesohyl cell. Scale bars: **a**, **b** 15 μm; **c** 10 μm

incomplete growing RM (~ 24–36 hpo) violates the regeneration process: RM stops growing and then gradually shrinks to the wound periphery (see Online Resource 10).

Mesohyl cell dynamics in the regenerative membrane

Time-lapse visualisation allows us to track individual mesohyl cells in the RM during its growth and transformation (Fig. 8; see Online Resources 6 and 8). All these cells tend to concentrate on the leading edge of the RM (Fig. 8a, b) and fall into three categories according to their morphology.

Cells of the two categories clearly correspond to the mesohyl cell types of intact body wall according to their appearance and behaviour. The first type are granular cells. Their cell surface looks like it continuously undergoes 'blebbing' (Fig. 8d, h, k). The number of granular cells in the RM is noticeably higher than in the intact body wall. The second type is represented by large amoebocytes. The long branching extensions are visible quite clearly in these cells which tend to migrate using these extensions (Fig. 8e, i).

The last and the most abundant type are small (5–7 μm in diameter) cells with amoeboid morphology. They usually have long (up to 2–4 cell diameters) and thin filopodia (~ 5–10 per cell) (Fig. 8c, f, g, j). We cannot directly match these cells with any cell type of the intact mesohyl. Yet at the later stage of regeneration, some of these cells

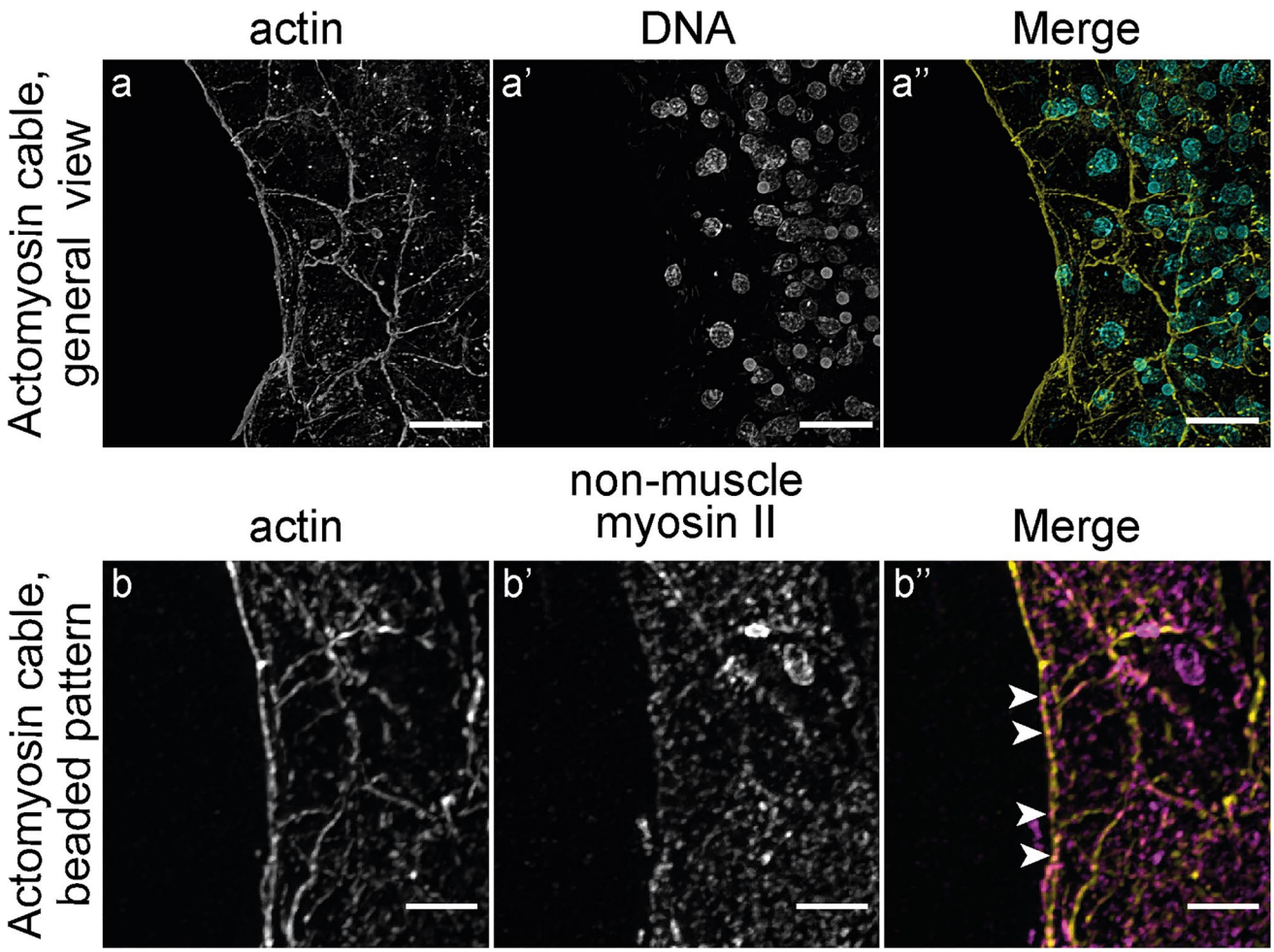

Fig. 7 Actomyosin contractile cable at the leading edge of the regenerative membrane (RM). **a** General view, 2.5% GlA in PBS fixation; **b** beaded intermittent pattern of myosin/actin co-localisation, ice-cold MeOH and then 4% PFA in PBS fixation; CLSM (maximum intensity projection of several focal planes); cyan – DNA, DAPI; yellow – actin filaments, antibody staining; magenta – non-muscle myosin II, antibody staining. The white arrowheads mark intermittent beaded pattern of myosin distribution. Scale bars: **a** 10 µm; **b** 5 µm

form tight groups where new spicules are synthesised (see Online Resources 6 and 8). Therefore, we assume that at least some of the cells with amoeboid morphology are freely migrating sclerocytes.

Mesohyl cell migration dynamics does not differ statistically between different cell types, so here we present generalised data. The average cell speed during the regeneration is 3.279 ± 0.0917 µm/min ($n = 68$). The migration efficiency of mesohyl cells is 0.5242 ± 0.0247 ($n = 70$).

The morphological parameters of the cells change during regeneration

As RM growth is considered to be dependent on the transformations of epithelial-like cell layers (Korotkova 1963; Lavrov et al. 2018; Caglar et al. 2021), we sought to estimate this process quantitatively. We describe the cell morphology in epithelial-like layers in the intact body wall and the RM, using three parameters: area, circularity, and aspect ratio.

The intact choanocytes are small cells with an area of 29.74 ± 0.515 µm^2 ($n = 131$) (Fig. 9a). These prismatic cells are almost round in the cross-section, so the circularity value is 0.907 ± 0.004 ($n = 131$) (Fig. 9b), and AR is 1.177 ± 0.008 ($n = 129$) (Fig. 9c).

Transdifferentiation of choanocytes to endopinacocytes results in a significant area increase (Fig. 9a) – 89.63 ± 7.535 µm^2 ($n = 50$, p-value $= 2.60e^{-31}$, Dunn's multiple comparisons test with Benjamini and Hochberg correction, or 'BH'), AR increase (Fig. 9c) up to 1.56 ± 0.049 ($n = 51$, p-value $= 8.09e^{-16}$, Dunn's multiple comparisons test with BH), and circularity decrease (0.65 ± 0.019, $n = 52$, p-value $= 1.25e^{-32}$, Dunn's multiple comparisons test with BH) (Fig. 9b).

Redifferentiating choanocytes at the later stages of regeneration have intermediate morphological parameters,

which distinguish them from both intact choanocytes and membrane endopinacocytes. They have a rather high area value of 62.04 ± 0.890 μm^2 (n = 285), significantly different (p-value = 4.26e^{-54}, Dunn's multiple comparisons test with BH) from intact choanocytes (Fig. 9a). They also differ in the circularity value (0.881 ± 0.002, n = 245) (Fig. 9b) and AR (1.226 ± 0.009, n = 276) (Fig. 9c) both from choanocytes (p-value = 1.03e^{-10} for circularity; p-value = 4.54e^{-3} for AR, Dunn's multiple comparison test with BH) and endopinacocytes (p-value = 2.71e^{-17} for circularity; p-value = 7.22e^{-12} for AR, Dunn's multiple comparisons test with BH).

Intact exopinacocytes have large (199.6 ± 5.188 μm^2, n = 266) (Fig. 9d) cytoplasmic plates with high circularity value (0.675 ± 0.006, n = 268) (Fig. 9e). The AR value of the plates (1.514 ± 0.019, n = 256) (Fig. 9f) indicates that the exopinacoderm is a stable cell layer and does not migrate in the intact body wall. The bodies of exopinacocytes merged into mesohyl has medium-size cell area (67.01 ± 1.941 μm^2, n = 73) with low circularity rate (0.128 ± 0.008, n = 67) and low AR (1.547 ± 0.037, n = 67).

As the exopinacocytes flatten during the regeneration, their cell area significantly increases (p-value = 1.994e^{-04}, two-tailed Mann-Whitney U-test) up to 231.2 ± 6.367 μm^2 (n = 196) (Fig. 9d). Notably, the circularity of cells significantly decreases to 0.629 ± 0.008 (Fig. 9e) (n = 196, p-value = 1.589e^{-05}, two-tailed Mann-Whitney U-test). The increase of AR value (1.587 ± 0.027, n = 185) is not statistically significant (p-value = 0.0771, two-tailed Mann-Whitney U-test) (Fig. 9f).

Discussion

The regeneration process in the calcareous sponge *Leucosolenia variabilis*

The regeneration in *L. variabilis* closely resembles similar process in bilaterian animals (Carlson 2007), and could be split into generalised steps: wound healing, mobilisation of cell precursors, and morphogenesis (Tiozzo and Copley 2015; Bideau et al. 2021).

The isolation of the internal milieu during *L. variabilis* regeneration corresponds to the wound healing step. It starts already at 1 hpo (see Online Resource 11) when leader cells of exopinacoderm spread and extend their filopodia to contact with transdifferentiating choanocytes over the mesohyl layer (Lavrov et al. 2018). This process helps restoring the barrier against pathogens and prevents osmotic shock. These cell shape changes are known to be transcription-independent, which is why they appear quickly after wounding (Cordeiro and Jacinto 2013).

The next step, the mobilisation of cell precursors, seems to be the key one, as it partially specifies the following morphogenesis type (Kawamura et al. 2008; Jopling et al. 2011; Gemberling et al. 2013). There are three main cell sources in regeneration: (1) proliferation and differentiation of adult stem cells, (2) dedifferentiation or transdifferentiation of somatic cells in an injured area, (3) proliferation of pre-existing fully differentiated somatic cells (Tiozzo and Copley 2015). These sources are not self-exclusive and could coexist in various combinations in some species. The following morphogenesis which leads to the reconstruction of lost body part could be epithelial or mesenchymal. The former type is based on transformations of epithelial cell layers in an injured area with minor or no contribution of cell proliferation. Mesenchymal morphogenesis, on the other hand, assumes blastema formation through intensive proliferation of mesenchymal cells undergoing the EMT and MET (Hay and Zuk 1995; Vervoort 2011; Borisenko et al. 2015; Alibardi 2022; Tang et al. 2022).

In the case of calcareous sponge regeneration, the mobilisation of cell precursors and subsequent morphogenesis appear to be merged into a single phase, the formation of RM. It is the main and unique process during regeneration in a calcareous sponges. RM grows due to spreading of two epithelial-like cell layers — exopinacoderm and choanoderm — over the wound orifice without any underlining substrate/ECM matrix. RM formation and its subsequent transformation into intact body wall do now require formation of blastemal-like accumulations of cells, what is characteristic reparative regeneration in Demospongiae (Borisenko et al. 2015; Ereskovsky et al. 2020).

The body wall regeneration in *L. variabilis* does not rely on the cell proliferation as well: there are no changes in number and distribution pattern of the proliferating cells in tissues adjacent and distant from the wound (Lavrov et al. 2018). Such situation seems to be typical for the regeneration processes in sponges (Borisenko et al. 2015; Ereskovsky et al. 2015, 2020; Caglar et al. 2021), and some authors assume that proliferation, as the main physiological mechanism of cell renewal in the aquiferous system, is suppressed during regeneration in sponges (Alexander et al. 2015; Borisenko et al. 2015; Melnikov et al. 2022).

Thus, the RM formation in *L. variabilis* is likely morphallactic process relying on the transformations of pre-existing cell layers through the epithelial morphogenesis. In this study, we aimed to trace cytoskeletal rearrangements underlying these morphological changes in the cells.

The dynamics of regenerative membrane formation

The dynamics of RM formations has three key features: it is non-linear, stochastic (display growth fluctuations), and varies greatly among individuals. In the process of RM formation, there are periods when there is much slower

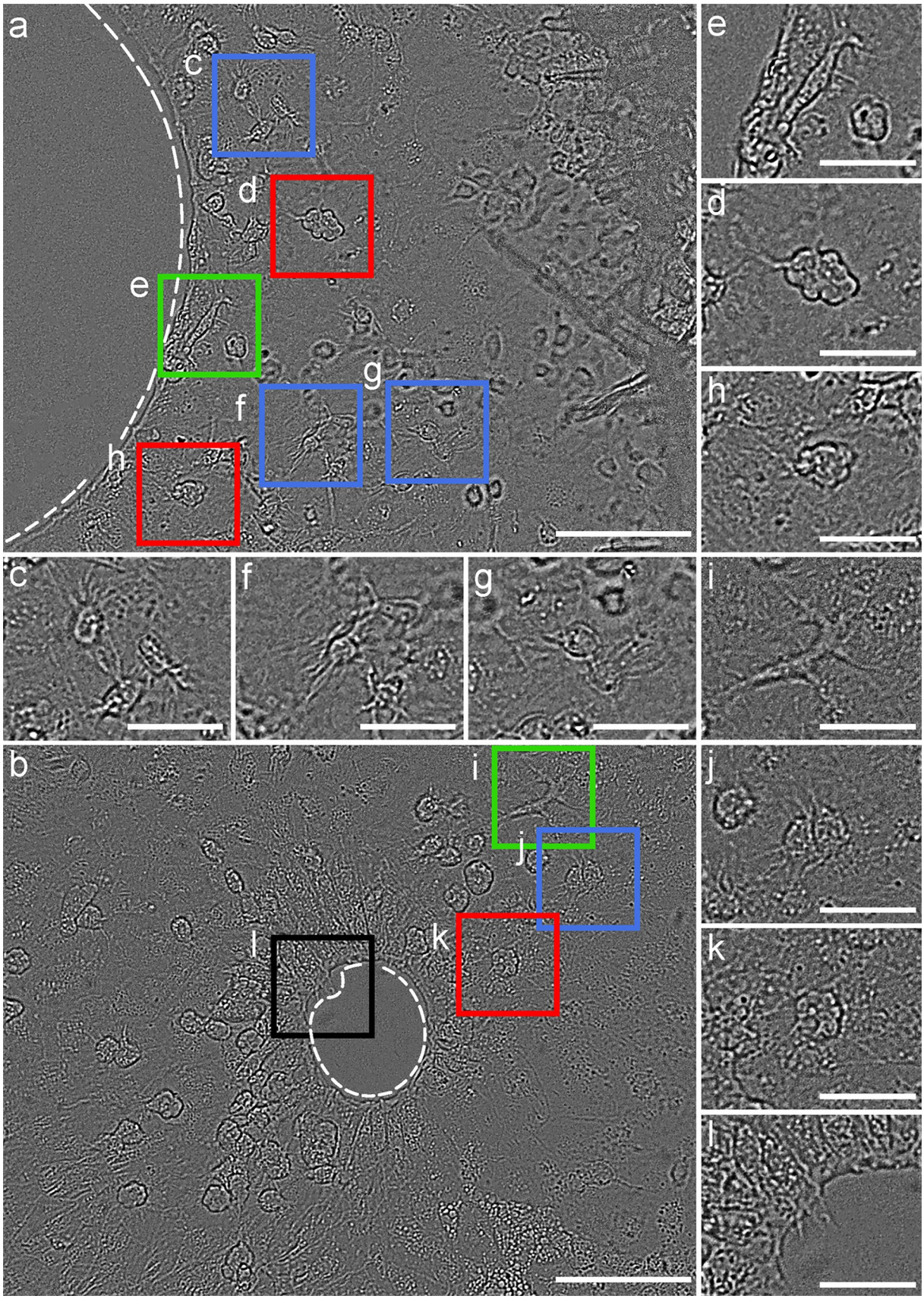

◂**Fig. 8** Mesohyl cells in the regenerative membrane (RM). **a**, **b** RM during closure, light microscopy; **c**, **f**, **g**, **j** sclerocytes (blue frames); **d**, **h**, **k** granular cells (red frames); **e**, **i** large amoebocytes (green frames); **l** filopodia on the leading edge of the RM (black frame). Light microscopy, frames from time-lapse imaging. White dotted lines mark the leading edge of the RM. Scale bars: **a**, **b** 50 µm; **c**–**l** 20 µm

dynamics than in the main phase of growth. First of them is an initial lag period between end of wound healing (~ 1 hpo) and the first appearance of RM on the periphery of the wound, which occurs only after ~ 12 hpo. A similar lag period of 6 h was observed during regeneration in the mouse corneal epithelium and was presumably associated with the reorganisation of cells at the leading edge (Danjo and Gipson 1998). Another period of slower dynamics occurs at later stages of RM growth and explains the non-linear nature of curves in Fig. 5f. We associate it with a decrease in the perimeter of the wound and, accordingly, contact inhibition, which is triggered by the membrane cells coming into contact, similar to how it occurs in cell monolayers (Lanosa and Colombo 2008). We also assume that the filopodia that appear in the cells of the RM leading edge (pinacocytes) might modulate this process similar to those involved in *Drosophila* dorsal closure. In that model, filopodia and lamellipodia on the opposite leading edges contact and draw cells together (Jacinto et al. 2000; Garcia-Fernandez et al. 2009).

The observed fluctuations in the dynamics of RM growth can be explained by the mechanical stress to which the leading edge of RM is subjected: time-lapse imaging allows to visualise tears occurring at the edge indicating the mechanical tension applied to the RM. Such tears cause a local retraction of the leading edge and, thus, temporary increase in the area of the wound. Similar observations were obtained in MDCK cells in a model of non-adhesive epithelization, where the wound in the monolayer was tightened by a stochastic sequence of contractions and increases in its area, and the observed amplitudes were up to 1/5 of the entire wound size (Nier et al. 2015).

We assume that the heterogeneity of dynamics among individual specimens is caused by different physiological states, the initial area of the wound, the conditions of the environment from which the animal was taken (atmospheric pressure, the strength of tidal influences, water temperature, season). It is known, for example, that the physiological state of sponges is affected by the temperature of the environment; its significant increase results in the mass death of individuals (Ereskovsky et al. 2019). The physiological state of an individual in turn directly affects the course of various restorative processes in sponges (Valisano et al. 2006; Lavrov et al. 2020; Ereskovsky et al. 2021).

Mesohyl cells: morphology and contribution to regeneration

Unlike pinacoderm and choanoderm, mesohyl is structureless; its cells are constantly moving and do not form any stable conglomerates. Mesohyl cells vary in morphology and perform multifarious functions in intact sponge tissues. Mesohyl of *L. variabilis* contains rather few cells both in terms of overall cell number and variety of cell types (Fig. 10c–e).

The role of sclerocytes, which are spicule-synthesising cells, seems to be the clearest and the most studied one. These cells form tight groups for extracellular synthesis of carbonate spicules. Sclerocytes have well-established septate junctions (Ledger 1975; Lavrov et al. 2018) which probably perform a barrier function, maintaining the ionic gradient between the extracellular spicule cavity and the mesohyl matrix. Sclerocytes have thick actin bundles outlining cell edges. This is consistent with the evidence that septate junctions are associated with actin filaments (Lane and Flores 1988).

Granular cells are found for the first time for *Leucosolenia* species. The reason for the homogeneous staining of the granular component is not clear and requires further research using other methods and dyes. The exact function of granular cells in *L. variabilis* is not established, but considering sponges in general, granular cells are attributed to the storage functions, chemical defence, antimicrobial activity, or reproduction process (Simpson 1984; Krylova et al. 2004; Gauthier 2009; Ternon et al. 2016; Ereskovsky and Lavrov 2021). Taking into account seasonal changes in number of granular cells in *L. variabilis* mesohyl, which increase in autumn and winter, it could be assumed that these cells may have a storage function.

Large amoebocytes remain an enigma since it is the first time such cells are found in sponge tissues. The most morphologically similar cell type is fiber cells in *Trichoplax adhaerens* which also have numerous long branching extensions. In Placozoa, these cells connect the ventral and dorsal epithelia to each other (Smith et al. 2014) and have a dense meshwork of actin filaments, probably providing them with ability to contract (Behrendt et al. 1986; Thiemann and Ruthmann 1989). However, the exact function of fiber cells remains unclear (Smith et al. 2014). As large amoebocytes of *L. variabilis* always lie above the choanoderm, we assume they could provide some kind of support for choanocytes either signal or mechanical. Or vice versa, large amoebocytes transmit signals and (or) nutritional chemicals from the choanoderm to other cells. Further research are required to clarify the occurrence of large amoebocyte in other sponge species and to evaluate their function.

The RM mesohyl forms a continuity with the mesohyl of intact body walls allowing free migration of mesohyl

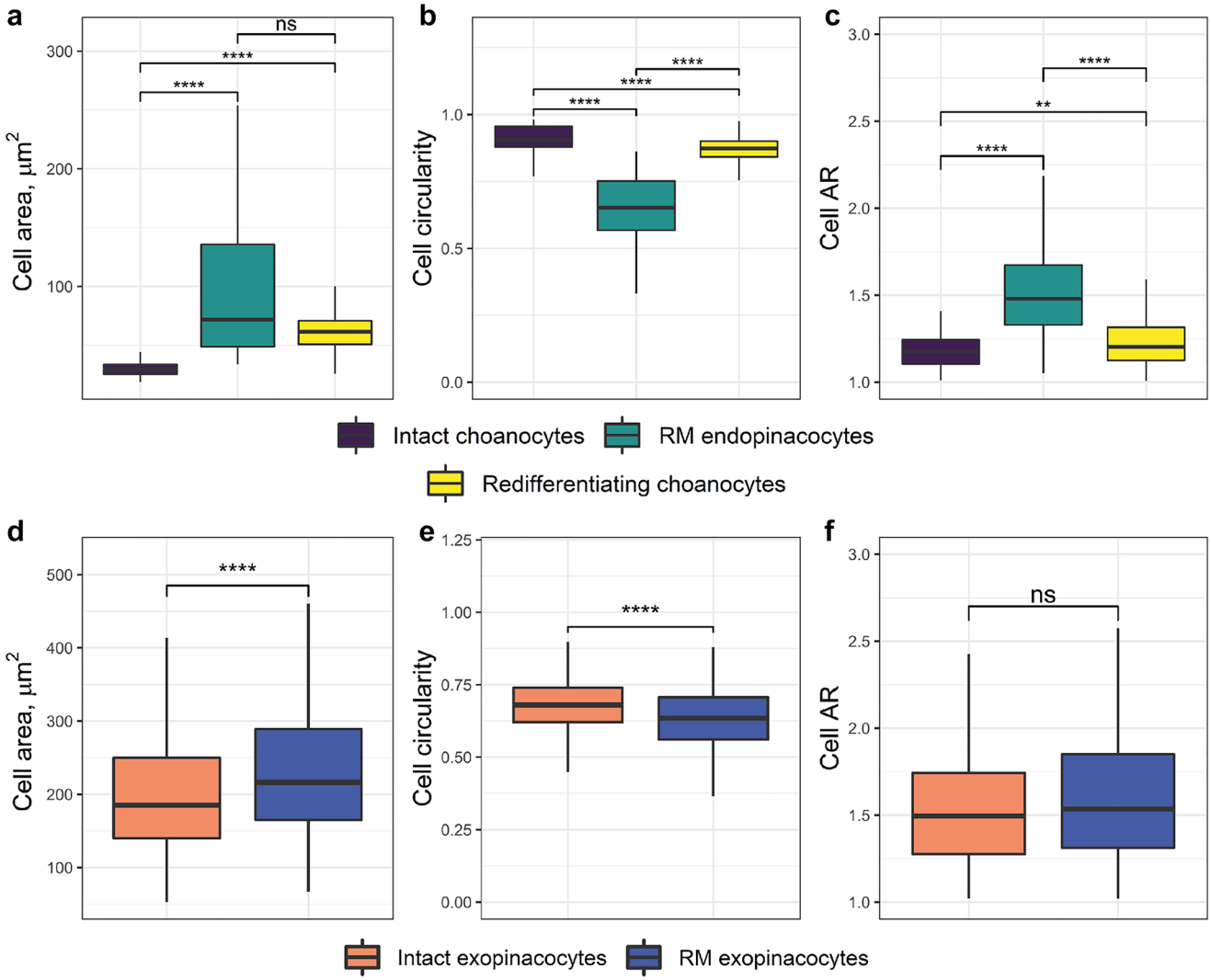

Fig. 9 Morphometrical analysis of cell transformations in the choanoderm (**a**–**c**) and exopinacoderm (**d**, **e**) during regenerative membrane formation. **a**, **d** Cell area, **b**, **e** circularity, and **c**, **f** aspect ratio. Data is shown with median values (thick horizontal lines), interquartile ranges (boxes) and total ranges (whiskers). Asterisks mark statistical significance between different cell types: $p < 0.0001$ (****); $p < 0.001$ (***); $p < 0.01$(**); $p < 0.05$ (*); ns, not significant. Dunn's post hoc tests with the Benjamin-Hochberg adjustment (**a**–**c**); the two-sided Mann-Whitney *U*-test (**d**, **e**)

cells. We were able to detect large amoebocytes and granular cells in RM, similar to those detected in intact body wall (Fig. 10c and d). However, the most numerous mesohyl cells of RM are cells with amoeboid morphology (Fig. 10e). The identity of these cells is not yet clear: some of them are probably migrating sclerocytes since cells with amoeboid morphology tend to associate with newly formed spicules; however, there is a possibility that some of these cells represent another cell type (Fig. 10e), which we are not able to detect in intact body wall due to their overall resemblance to exopinacocyte bodies.

At the moment, it seems that mesohyl cells do not directly participate in the most active stage of *L. variabilis* regeneration—RM formation. Ultrastructural studies have not revealed the contribution of mesohyl cells to RM formation (Lavrov et al. 2018; Ereskovsky et al. 2021). However, our time-lapse imaging illustrates that mesohyl cells tend to concentrate at the leading edge of the RM. Possibly, this is a way to intensify ECM synthesis in the forming tissue, since mesohyl cells generally have this function in sponge tissues (Ereskovsky 2010; Ereskovsky and Lavrov 2021).

Another sign of the involvement of mesohyl cells in regeneration process in *L. variabilis* is increased number of the granular cell in RM. Considering a possible storage function of granular cells in *L. variabilis*, these cells might transport nutrients necessary for the regeneration or substances

with antimicrobial activity preventing exceed development of microorganisms at the wound site. Similar increase (~2–3 times) of spherulous cell number was shown for the epithelization stage of regeneration in demosponge *Aplysina cavernicola*. In this case, the authors suggest that the contents of inclusions in these cells can perform an antibacterial function, thereby protecting the wound surface from pathogenic microorganisms (Ereskovsky et al. 2020). Another example is grey cells in *Polymastia mamillaris*. They are cells with inclusions involved in the glycogen metabolism (Boury-Esnault 1977). During regeneration, grey cells actively migrate towards the wound, increase their glycogen content, and possibly in such a way deliver nutrients required to cover energetic demands of regeneration (Boury-Esnault 1976).

Finally, sclerocytes are directly involved in the regeneration during the stage of RM transformation into intact body wall, as they synthesise new spicules in transforming RM.

Porocytes, tubular cells through which water penetrates from the external environment to the spongocoel, are not considered to be mesohyl cells, but will be discussed here as they are not directly involved in the formation of RM. Porocytes of calcareous sponges are capable of contracting and, therefore, regulating water flow through the animal body (Jones 1966; Eerkes-Medrano and Leys 2006). The actin cytoskeleton of porocytes forms a widely spaced grid and may fit to constant contractions. This assumption seems especially relevant due to the establishment of contractile actin bundles that contain striated muscle myosin II and are regulated by myosin light-chain kinase (MLCK) in the sponge *Ephydatia muelleri* tissues (Colgren and Nichols 2022).

During regeneration, porocytes appear synchronously with redifferentiation choanocytes, from the periphery of the RM to its centre. In this work, we did not track the source of these cells, but in an earlier study it was shown that porocytes are the result of the transdifferentiation of RM exopinacocytes (Lavrov et al. 2018) (Fig. 10a).

In vivo studies of behaviour and functions of mesohyl cells are hindered in sponges. Even in thin-walled *L. variabilis*, direct observation of mesohyl cells is impossible due to dense net of spicules. Such methodological issues at least partially cause absence of consistent view on diversity and functions of mesohyl cells in sponges. In such a case, RM could become a useful model for in vivo studies of mesohyl in calcareous sponges. We believe that RM mesohyl (especially after formation of the complete RM) could be considered a reasonable approximation of intact state of sponge mesohyl: many aspects of behaviour of mesohyl cells in RM may reflect their functions in intact sponge tissues.

Similarly, in the case of porocyte, complete RM gives an opportunity to directly access the cellular source of this cell type, as well as directly observe behaviour of porocytes under control laboratory conditions.

RM formation as a result of epithelial morphogenetic processes

The pinacoderm in asconoid sponges forms the outer cover of the body (exopinacoderm) and outlines the inner part of the oscular rim (endopinacoderm) (Bergquist 1978; Eerkes-Medrano and Leys 2006; Ereskovsky and Lavrov 2021). In *L. variabilis*, intact exopinacocytes are T-shaped (Fig. 10a). Such type of organisation (called 'insunk epithelium') is also present in many Demospongiae species (Simpson 1984) and in some species from other phyla: epithelium of *Convoluta convoluta* (Xenacoelomorpha) (Pedersen 1964), epithelium of some lecithoepitheliates and bdellourid triclads (Tyler and Hooge 2004), and dorsal epithelial cells in *Trichoplax adhaerens* (Placozoa) (Smith et al. 2014). Therefore, such morphology is not unique and is probably associated with a certain plasticity of the epithelial tissues.

And yet intact *L. variabilis* exopinacocytes have a unique feature, reported for the first time in our work: filopodial extensions connecting cell bodies with each other (Fig. 10a). We are not well aware what function these extensions fulfil; still, there are some assumptions. First, they might provide mechanical integrity and stability of the cell layer as there is no evidence of conventional cell–cell junctions between cytoplasmic plates, though there are many studies confirming the presence of cell adhesion machinery in sponges (Boury-Esnault et al. 2003; Adell et al. 2004; Leys et al. 2009; Leys and Hill 2012; Leys and Riesgo 2012; Jonusaite et al. 2016; Belahbib et al. 2018; Mitchell and Nichols 2019). Second assumption is that extensions connecting exopinacocytes provide signalling and temporally and spatially coordinated contraction of exopinacoderm and, thus, regulate water flow through the body, similar to previously observed (Jones 1957; Elliott and Leys 2007; Nickel et al. 2011).

The outer layer of RM consists of flat polygonal exopinacocytes (Fig. 10a). These cells represent a result of fusion between cytoplasmic plate and cell body of exopinacocytes. We consider this transformation as a deep change of cell shape due to participation in morphogenetic process, but not as de-/transdifferentiation as exopinacocytes do not change their functional role. Transformation of exopinacocytes accompanied by substantial changes in actin cytoskeleton structure. In exopinacocytes on the leading edge of RM, cortical actin bundles are replaced by filopodia on the wound side, while remain stable at the other sides of the cells (Fig. 7a). These either mechanosensing or signalling protruding structures probably perform a similar function as was shown in *Drosophila* dorsal closure—sealing the opposite edges of epithelium (Stramer et al. 2005; Garcia-Fernandez et al. 2009; Abreu-Blanco et al. 2012). The same cells (pinacocytes sensu lato) form an actomyosin cable on the leading edge of RM.

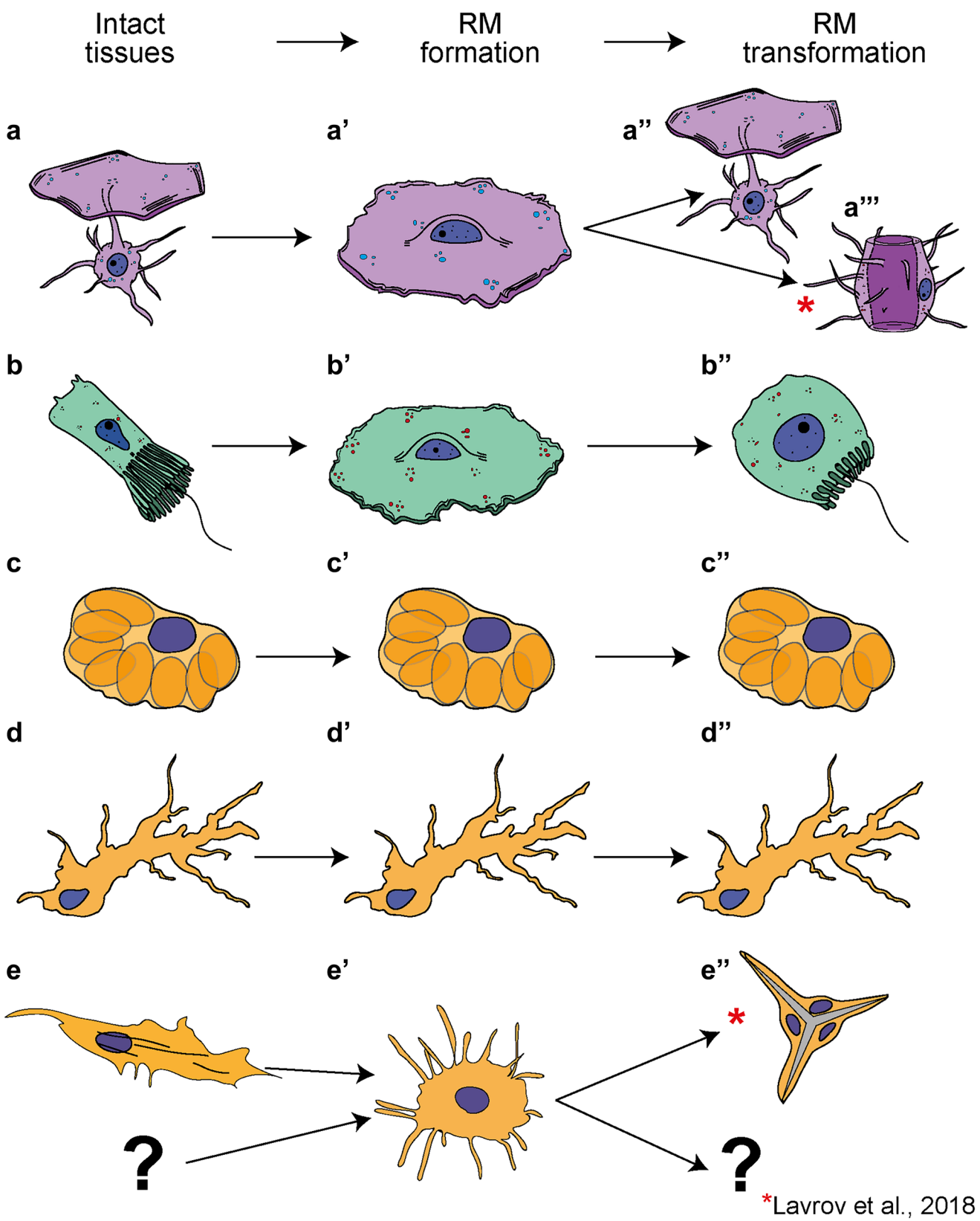

◂**Fig. 10** Diagram of cell transformations during regeneration in ring-like body fragment of the calcareous sponge *L. variabilis*. **a** Exopinacoderm cell lineage transformations: **a** intact exopinacocyte, **a′** exopinacocyte of RM; **a″** exopinacocyte of transformed RM, **a‴** porocyte, derived from RM exopinacocyte; **b** choanoderm cell lineage transformations: **b** intact choanocyte, **b′** endopinacocytes of RM, **b″** redifferentiating choanocyte; **c**–**e** mesohyl cell types transformations: **c**–**c″** granular cell transformation, **d**–**d″** large amoebocyte transformation, **e** intact sclerocytes, **e′** cell with amoeboid morphology of RM, **e″** spicule's synthesis by sclerocytes during RM transformation. The question mark (?) indicates possibly existing another mesohyl cell type which we are not able to distinguish properly; red asterisk mark (*) indicates data gained from previous study (Lavrov et al. 2018)

Our morphometric analysis indicates that flattening of the exopinacocytes during RM formation leads to the increase in cell area, as well as to the polarisation in the epithelial-like cell layer of exopinacoderm, as cell circularity decreases and AR increases. However, there are no common or predicted migratory structures (lamellipodia, filopodia, or lobopodia), and no other features of collective cell crawling detected. During flattening, exopinacocytes do not lose intercellular junctions, they move collectively, though there are no leader cells typical for the collective cell migration mechanism of epithelization (Reffay et al. 2014). We also did not observe cryptic lamellipodia in cells of the second, third, and more distant rows from the leading edge, although it has been shown that such structures might contribute to collective cell migration (Farooqui and Fenteany 2005). We assume that the decrease in circularity is caused by the appearance of filopodia and the cell elongation towards the wound centre. This as well explains the observed AR changes. We also associate cell elongation with mechanical tension generated by actomyosin cable contraction, as previously shown in cell monolayer epithelization (Lee and Gotlieb 2005; Anon et al. 2012) and *Drosophila* embryogenesis (Jankovics and Brunner 2006; Garcia-Fernandez et al. 2009). Hereby, morphological changes of individual exopinacocytes indicate fundamental transformations of the epithelial-like cell layer of the exopinacoderm.

The choanoderm in the asconoid body of *L. variabilis* represents the inner layer of cells (Fig. 10b). It provides feeding, excretion, oxygenation, and gametogenesis (Simpson 1984). The general appearance of choanoderm in Calcarea and Demospongiae includes clear apicobasal polarity and structures similar to cell junctions (Eerkes-Medrano and Leys 2006; Lavrov et al. 2018, 2022). Choanocytes contains orthologous proteins of cellular junction (Leys and Hill 2012; Peña et al. 2016; Miller et al. 2018; Mitchell and Nichols 2019) and basal lamina (Boute et al. 1996; Fahey and Degnan 2010; Leys and Riesgo 2012). These data provide strong evidence for claiming choanoderm in Calcarea and Demospongiae as epithelial-like cell layer. This assertion is confirmed by subcellular cytoskeletal organisation of choanocytes provided in this study. The actin cytoskeleton in choanocytes is quite similar to those reported in prismatic epithelia of Eumetazoa (Bretscher and Weber 1978; Kukulies et al. 1984; Waterman-Storer et al. 2000): actin bundles act as microvilli core and are oriented along the apicobasal axis of the cells.

It is generally accepted to call transformations of sponge cells transdifferentiation since cells completely change their morphological appearance and functional role (Borisenko et al. 2015; Ereskovsky et al. 2015; Adamska 2018; Lavrov et al. 2018; Caglar et al. 2021). Therefore, transformation of choanocytes with loss of main morphological features (prismatic shape, microvilli collar, and flagellum) following by the loss of filtering ability can also be considered a transdifferentiation.

The flattening of originally prismatic choanocytes (accompanied by cell area increase, circularity decrease, and AR increase) provides a source (together with exopinacocytes) for covering the excised area (Fig. 10b). Similar morphological changes are observed during intestinal epithelial restitution (Tétreault et al. 2005). Furthermore, such strong changes are only possible due to fundamental rearrangements of the cytoskeleton. For example, during *Drosophila* development, cells of amnioserosa flatten end elongate autonomously by so-called rotary cell elongation (Pope and Harris 2008). This mechanism relies on coordinated reorganisation of both microtubules and actin filaments without disruption of cell junctions. Transdifferentiation of choanocytes probably follows the same route considering the observed morphological changes. Similarly to the exopinacoderm of growing RM, we did not observe structures responsible for the cell layer migration or any leader cells in the endopinacoderm.

The reverse process, columnarisation of flat endopinacocytes and restoration of choanocyte morphological characteristics (Fig. 10b), is referred here as redifferentiation as in previous studies (Lavrov et al. 2018; Ereskovsky et al. 2020). During redifferentiation endopinacocytes become spherical and, correspondingly, cell area and AR decrease, while circularity increases. Later stages are accompanied by further apicobasal elongation of cells (Lavrov et al. 2018). This process resembles terminal differentiation of kidney epithelia, when (1) cells establish terminal web and brush-border microvilli on the apical side, (2) their nuclei move to a basal cell side, and (3) cells acquire a columnar shape (Vijayakumar et al. 1999). There is no evidence of the existence of a terminal web in choanocytes, probably due to poor actin preservation during the preparation of TEM samples. However, other listed morphological features specific to these cells are present and become evident during the transformation of RM into the body wall (Fig. 10b).

Interestingly, the microvilli collar and the flagellum are the last to be lost during transdifferentiation and the first to

re-establish during redifferentiation. Since the main function of choanocytes is water filtration, such timings can be interpreted as an adaptation: it allows choanocytes to partially perform the main function even with an altered filtration apparatus.

Cell transformations during RM formation are fundamentally similar to those characteristics of bilaterian animals, at least at the level of cell morphology and actin filament rearrangements. Thus, we assume that regeneration in *L. variabilis* is driven by epithelial morphogenesis with some distinct features: the absence of a substrate for cell movement and the presence of actin cable at the leading edge of the RM.

RM formation as an analogue of epithelization over a non-adhesive substrate

Epithelial healing is based on two interacting mechanisms: collective cell crawling and actin 'purse-string' contraction. It was widely accepted that the first mechanism is more peculiar for adult animals (Zahm et al. 1991, 1997; Nusrat et al. 1992; Yin et al. 2008) and the second one is typical for embryonic wounds and development (Martin and Lewis 1992; Brock et al. 1996; Jacinto et al. 2000). Yet, at the moment, the number of works indicating these mechanisms work conjointly is increasing. Some researchers detect these mechanisms at different stages of the wound healing process (Brugués et al. 2014; Kuipers et al. 2014); others find them interacting throughout the time of healing process (Fenteany et al. 2000; Klarlund 2012; Richardson et al. 2016; Kamran et al. 2017). There are also studies debating if the mechanism is determined by the size and (or) geometry of the wound (Bement et al. 1993; Danjo and Gipson 1998; Grasso et al. 2007).

In the last few years, the model of 'non-adhesive epithelization' has arise. This model assumes the absence of an adhesive substrate at the site of a wound: cells are not allowed to spread, flatten, and migrate over the wound and therefore form so-called epithelial bridges stretched over a non-adhesive substrate (Vedula et al. 2014; Albert and Schwarz 2016). Their formation relies on the functioning of the actomyosin cable in cells from the 'bridge', connected not only to each other, but also to cells on an adhesive substrate around the wound site. The whole structure is also subjected to significant mechanical tension transmitted between neighbouring cells (Nier et al. 2015; Chen et al. 2019).

As was already mentioned, the RM formation occurs without a substrate; the membrane encloses over a gap in the sponge body wall. The morphology of RM is quite similar to the 'epithelial bridges' obtained by Vedula and co-authors (2014) during cultivating the MDCK line on fibronectin strips separated by a non-adhesive substrate. In that study, the formation of 'bridges' was slowed down if the distance between the fibronectin strips was increased to ~ 200 μm. However, our observations show that the formation of an actomyosin cable allows RM to overcome such distances with no issues and a wound with an initial radius of ~ 1000 μm can be rapidly sealed.

It is also known that epithelialization through the mechanism of actomyosin ring contraction requires the presence of cell–cell junction proteins which form clusters along the leading edge: cadherins (Brock et al. 1996; Danjo and Gipson 1998; Brugués et al. 2014; Vedula et al. 2014), ZO-1 (Bement et al. 1993; Brugués et al. 2014), vinculin (Grasso et al. 2007). Some of them affect actin cable stability: for example, monoclonal anti-E-cadherin antibodies (ECCD-1) disrupt wound healing by the purse-string mechanism in mouse corneal epithelium (Danjo and Gipson 1998). This additionally convinces us that there should be cell junctions between sponge cells that resemble those belonging to Eumetazoans, but they may differ in morphology and protein composition. In consistence with this evidence, there are studies indicating orthologous cell–cell junction proteins in sponge tissues (Boury-Esnault et al. 2003; Adell et al. 2004; Eerkes-Medrano and Leys 2006; Leys and Riesgo 2012; Miller et al. 2018). The presence of cell junctions is driven by the necessity of stabilisation of the actin cable, subjected to significant mechanical tension. Disruptions and subsequent retractions of the RM leading edge, in addition to the already mentioned tension, might be a consequence of the force generated by the water flow through the body fragments. That is an additional obstacle to stabilising the actin cable.

The initial wound size and characteristic asymmetry of RM growth suggest we observe not a complete actomyosin cable formed along the entire perimeter of the wound (at least in the beginning), but shorter fragments ('actin arcs') as is typical for the epithelization of large wounds (Bement et al. 1993). Each of these fragments generates mechanical forces in its own sector of the RM.

The contractile abilities of the actomyosin cable at the leading edge of the wound are often confirmed by functional analysis. In this way, the addition of 100 μmol/l of blebbistatin to the SK-CO15 monolayers inhibited wound closure by approximately 50% (Babbin et al. 2009). For wounds in MDCK monolayers, myosin light chain is shown to concentrate in the basolateral part of the cell (area of protrusion formation) and in the apical region (area of actomyosin cable formation). In the presence of blebbistatin, myosin accumulation continues, protrusions continue to form, and yet the cable does not contract (Tamada et al. 2007). The adding of blebbistatin also inhibits wound closure over the non-adhesive substrates (Nier et al. 2015); still the effect is reversible (Chen et al. 2019). Similarly, in our functional experiments, the addition of 50 μM blebbistatin to the growing RM prevents its

subsequent growth, pointing to the dependence of the regeneration process in *L. variabilis* upon the contractile properties of the actomyosin cable on RM leading edge.

Summing up, we assume that the formation of a RM during the regeneration in *L. variabilis* depends mainly on the contractile activity of the actomyosin cable, which coordinates extension of the cell layers of the exopinacoderm and endopinacoderm (transdifferentiated choanoderm) to the centre of the wound, and ensures the direction and constancy of their movement in non-adhesive substrate conditions. However, the question about the origin of force pushing the leading edge of the cell layer towards the centre of the wound remains relevant (Fenteany et al. 2000; Anon et al. 2012). Some studies indicate the cell crawling as the main way for wound closure while actin cable functions as a guiding structure (Anon et al. 2012). Others suggest that actomyosin cable assembly and contraction draw adjacent edges of the wound together (Tamada et al. 2007; Vedula et al. 2015).

Conclusions

Regenerative membrane formation during regeneration in calcareous sponges is dependent on exopinacoderm and choanoderm coordinated flattening accompanied by the choanocyte transdifferentiation with temporary loss of the morphological features and physiological function. This process proceeds without a contribution of proliferation and, at some points, resembles 'non-adhesive epithelization': it has similar dynamics, occurs without substrate, and probably depends on the actomyosin cable formation and contraction. Morphological changes of the cells and alterations in their actin cytoskeleton are similar to those characteristic to Eumetazoans and, thus, are conservative through evolution.

Our data provide a basis for a further mechanistic analysis of morphogenesis in sponges. For example, the regulation of cytoskeleton components (actin filaments, microtubules) in sponges remains poorly characterised. This is also true for interactions and mutual regulation of microtubule systems and actin filaments, their role in morphogenetic processes. Forces driving RM formation and sealing also require further elucidation. The role of Rho family GTPases and their effector proteins as well as microtubules and their associated proteins in regeneration of calcareous sponges are promising areas for future studies. Investigations in this direction will be an important step towards describing the mechanisms of morphogenetic processes in the basal groups of multicellular animals and the role of the cytoskeleton in these processes, which is the basis for identifying the mechanisms establishing true tissues in evolution.

Abbreviations AR: Aspect ratio; CLSM: Confocal laser scanning microscopy; DAPI: 4′,6-Diamidino-2-phenylindole; ECM: Extracellular matrix; EMT: Epithelial-mesenchymal transition; FSW: Filtered seawater; GTPase: Nucleotide guanosine triphosphate (GTP) hydrolase; hpo: Hours post operation; MET: Mesenchymal-epithelial transition; MLCK: Myosin light-chain kinase; RM: Regenerative membrane; PBS: Phosphate-buffered saline

Supplementary Information The online version contains supplementary material available at https://doi.org/10.1007/s00441-023-03810-5.

Acknowledgements The authors acknowledge the support of Lomonosov Moscow State University Program of Development (Nikon A1 CLSM) and Centre of microscopy WSBS MSU. The authors sincerely thank Daniyal Saidov (Lomonosov Moscow State University) for statistical analysis tips, Elena Voronezhskaya (Koltzov Institute of Developmental Biology of Russian Academy of Sciences) for fixation recommendations, and Nikolay Melnikov, Anastasiia Kovaleva, Anna Tvorogova, Stanislav Kremnyov (Lomonosov Moscow State University), and Alexander Ereskovsky (Koltzov Institute of Developmental Biology of Russian Academy of Sciences) for helpful tips and advice.

Author contributions KS, AL, and AS designed the study. KS, AL, and FB collected the material, carried out CLSM cytoskeleton studies, and analysed and visualised the data. KS conducted experiments and performed statistical analysis and its visualisation as well as time-lapse imaging and its post-processing. AL, KS, and AS prepared the manuscript with contributions from all authors. All authors reviewed and approved the final manuscript.

Funding The research was supported by the Russian Foundation for Basic Research project no. 21-54-15006 and by Governmental Basic Research Program for the Koltzov Institute of Developmental Biology of the Russian Academy of Sciences no. 0088-2021-0009 (Kseniia Skorentseva).

Data availability Raw data were generated at Lomonosov Moscow State University, Faculty of Biology. Derived data supporting the findings of this study are available from the corresponding author Kseniia V. Skorentseva (skorentseva.ksenya.2016@post.bio.msu.ru) on request. Raw images used in this study are available in the Mendeley Data repository, https://data.mendeley.com/datasets/28g3jt3c22 (Figures, https://doi.org/10.17632/28g3jt3c22.1) and https://data.mendeley.com/datasets/s96kd597gr (Online Resources, https://doi.org/10.17632/s96kd597gr.1).

Declarations

Consent to participate Not applicable.

Conflict of interest The authors declare no competing interests.

References

Abreu-Blanco MT, Verboon JM, Liu R, Watts JJ, Parkhurstet SM (2012) *Drosophila* embryos close epithelial wounds using a combination of cellular protrusions and an actomyosin purse string. J Cell Sci 125:5984–5997. https://doi.org/10.1242/jcs.109066

Adamska M (2018) Differentiation and transdifferentiation of sponge cells. Results Probl Cell Differ 65:229–253. https://doi.org/10.1007/978-3-319-92486-1_12

Adell T, Gamulin V, Perović-Ottstadt S, Wiens M, Korzhev M, Muller IM, Muller WEG (2004) Evolution of metazoan cell junction proteins: the scaffold protein MAGI and the transmembrane receptor tetraspanin in the demosponge *Suberites domuncula*. J Mol Evol 59:41–50. https://doi.org/10.1007/s00239-004-2602-2

Albert PJ, Schwarz US (2016) Dynamics of cell ensembles on adhesive micropatterns: bridging the gap between single cell spreading and collective cell migration. PLoS Comput Biol 12:1–34. https://doi.org/10.1371/journal.pcbi.1004863

Alexander BE, Achlatis M, Osinga R, van der Geest HG, Cleutjens JPM, Schutte B, de Goeij JM (2015) Cell kinetics during regeneration in the sponge *Halisarca caerulea*: How local is the response to tissue damage? PeerJ 2015:1–19. https://doi.org/10.7717/peerj.820

Alibardi L (2022) Activation of cell adhesion molecules and Snail during epithelial to mesenchymal transition prior to formation of the regenerative tail blastema in lizards. J Exp Zool B Mol Dev Evol. https://doi.org/10.1002/JEZ.B.23139

Anon E, Serra-Picamal X, Hersen P, Gauthierc NC, Sheetz MP, Trepat X, Ladouxa B (2012) Cell crawling mediates collective cell migration to close undamaged epithelial gaps. Proc Natl Acad Sci USA 109:10891–10896. https://doi.org/10.1073/pnas.1117814109

Babbin BA, Koch S, Bachar M, Conti M-A, Parkos CA, Adelstein RS, Nusrat A, Ivanov AI (2009) Non-muscle myosin IIA differentially regulates intestinal epithelial cell restitution and matrix invasion. Am J Pathol 174:436–448. https://doi.org/10.2353/ajpath.2009.080171

Behrendt G, Ruthmann A, Behrendt G, Wahl R (1986) The ventral epithelium of *Trichoplax adhaerens* (Placozoa): cytoskeletal structures, teil contacts and endocytosis. Zoomorphology 200:123–130

Belahbib H, Renard E, Santini S, Jourda C, Claverie J-M, Borchiellini C, Le Bivic A (2018) New genomic data and analyses challenge the traditional vision of animal epithelium evolution. BMC Genomics 19:1–15. https://doi.org/10.1186/s12864-018-4715-9

Bement WM, Forscher P, Mooseker MS (1993) A novel cytoskeletal structure involved in purse string wound closure and cell polarity maintenance. J Cell Biol 121:565–578. https://doi.org/10.1083/jcb.121.3.565

Bergquist PR (1978) Sponges. University of California Press, Berkeley and Los Angeles

Bideau L, Kerner P, Hui J, Vervoort M, Gazave E (2021) Animal regeneration in the era of transcriptomics. Cell Mol Life Sci 78:3941–3956. https://doi.org/10.1007/s00018-021-03760-7

Borisenko IE, Adamska M, Tokina DB, Ereskovsky AV (2015) Transdifferentiation is a driving force of regeneration in *Halisarca dujardini* (Demospongiae, Porifera). PeerJ 3:e1211. https://doi.org/10.7717/peerj.1211

Boury-Esnault N (1976) Morphogenèse Expérimentale Des Papilles Inhalantes De L'éponge Polymastia Mamillaris (Muller). Arch Zool Exp Gén 117:181–196

Boury-Esnault N (1977) A cell type in sponges involved in the metabolism of glycogen. Cell Tissue Res 175:523–539

Boury-Esnault N, Ereskovsky A, Bézac C, Tokina D (2003) Larval development in the Homoscleromorpha. Invertebr Biol 122:187–202

Boute N, Exposito JY, Boury-Esnault N, Vacelet J, Noro N, Miyazaki K, Yoshizato K, Garrone R (1996) Type IV collagen in sponges, the missing link in basement membrane ubiquity. Biol Cell 88:37–44. https://doi.org/10.1016/S0248-4900(97)86829-3

Bretscher A, Weber K (1978) Localization of actin and microfilament-associated proteins in the microvilli and terminal web of the intestinal brush border by immunofluorescence microscopy. J Cell Biol 79:839–845. https://doi.org/10.1083/JCB.79.3.839

Brock J, Midwinter K, Lewis J, Martin P (1996) Healing of incisional wounds in the embryonic chick wing bud: characterization of the actin purse-string and demonstration of a requirement for Rho activation. J Cell Biol 135:1097–1107. https://doi.org/10.1083/jcb.135.4.1097

Brugués A, Anon E, Conte V, Veldhuis JH, Gupta M, Colombelli J, Muñoz JJ, Wayne Brodland G, Ladoux B, Trepat X (2014) Forces driving epithelial wound healing. Nat Phys 10:683–690. https://doi.org/10.1038/NPHYS3040

Caglar C, Ereskovsky A, Laplante M, Tokina D, Leininger S, Borisenko I, Aisbett G, Pan D, Adamski M, Adamska M (2021) Fast transcriptional activation of developmental signalling pathways during wound healing of the calcareous sponge *Sycon ciliatum*. bioRxiv. https://doi.org/10.1101/2021.07.22.453456

Carlson B (2007) Principles of regenerative biology. Elsevier, USA

Chen T, Callan-Jones A, Fedorov E, Ravasio A, Brugués A, Ong HT, Toyama Y, Low BC, Xavier Trepat X, Shemesh T, Voituriez R, Ladoux B (2019) Large-scale curvature sensing by directional actin flow drives cellular migration mode switching. Nat Phys 15:393–402. https://doi.org/10.1038/s41567-018-0383-6

Colgren J (2022) Nichols SA (2022) MRTF specifies a muscle-like contractile module in Porifera. Nat Commun 131(13):1–11. https://doi.org/10.1038/s41467-022-31756-9

Cordeiro JV, Jacinto A (2013) The role of transcription-independent damage signals in the initiation of epithelial wound healing. Nat Rev Mol Cell Biol 14:249–262. https://doi.org/10.1038/nrm3541

Danjo Y, Gipson IK (1998) Actin 'purse string' filaments are anchored by E-cadherin-mediated adherens junctions at the leading edge of the epithelial wound, providing coordinated cell movement. J Cell Sci 111:3323–3332. https://doi.org/10.1242/jcs.111.22.3323

Eerkes-Medrano DI, Leys SP (2006) Ultrastructure and embryonic development of a syconoid calcareous sponge. Invertebr Biol 125:177–194. https://doi.org/10.1111/j.1744-7410.2006.00051.x

Elliott GRD, Leys SP (2007) Coordinated contractions effectively expel water from the aquiferous system of a freshwater sponge. J Exp Biol 210:3736–3748. https://doi.org/10.1242/jeb.003392

Ereskovsky A, Lavrov A (2021) Porifera. In: Invertebrate histology. Wiley, pp 19–54

Ereskovsky AV (2010) The comparative embryology of sponges. Springer, Netherlands

Ereskovsky AV, Borisenko IE, Bolshakov FV, Lavrov AI (2021) Whole-body regeneration in sponges: diversity, fine mechanisms, and future prospects. Genes (basel). https://doi.org/10.3390/GENES12040506

Ereskovsky AV, Borisenko IE, Lapébie P, Gazave E, Tokina DB, Borchiellini C (2015) *Oscarella lobularis* (Homoscleromorpha, Porifera) regeneration: epithelial morphogenesis and metaplasia. PLoS ONE 10:1–28. https://doi.org/10.1371/journal.pone.0134566

Ereskovsky AV, Lavrov AI, Bolshakov FV, Tokina DB (2017) Regeneration in White Sea sponge Leucosolenia complicata (Porifera, Calcarea). Invertebr Zool 14:108–113. https://doi.org/10.15298/invertzool.14.2.02

Ereskovsky AV, Ozerov DA, Pantyulin AN, Tzetlin AB (2019) Mass mortality event of White Sea sponges as the result of high temperature in summer 2018. Polar Biol 42:2313–2318. https://doi.org/10.1007/S00300-019-02606-0

Ereskovsky AV, Tokina DB, Saidov DM, Baghdiguian S, Le Goff E, Lavrov AI (2020) Transdifferentiation and mesenchymal-to-epithelial transition during regeneration in Demospongiae (Porifera). J Exp Zool Part B Mol Dev Evol 334:37–58. https://doi.org/10.1002/jez.b.22919

Fahey B, Degnan BM (2010) Origin of animal epithelia: insights from the sponge genome. Evol Dev 12:601–617. https://doi.org/10.1111/j.1525-142X.2010.00445.x

Farooqui R, Fenteany G (2005) Multiple rows of cells behind an epithelial wound edge extend cryptic lamellipodia to collectively drive cell-sheet movement. J Cell Sci 118:51–63. https://doi.org/10.1242/jcs.01577

Fenteany G, Janmey PA, Stossel TP (2000) Signaling pathways and cell mechanics involved in wound closure by epithelial cell sheets. Curr Biol 10:831–838. https://doi.org/10.1016/S0960-9822(00)00579-0

Gaino E, Magnino G (1999) Dissociated cells of the calcareous sponge *Clathrina*: a model for investigating cell adhesion and cell motility in vitro. Microsc Res Tech 44:279–292

Garcia-Fernandez B, Campos I, Geiger J, Santos AC, Jacinto A (2009) Epithelial resealing. Int J Dev Biol 53:1549–1556. https://doi.org/10.1387/ijdb.072308bg

Gauthier M (2009) Developing a sense of self: exploring the evolution of immune and allorecognition mechanisms in metazoans using the demosponge *Amphimedon queenslandica*. Phd Thesis, School of Biological Sciences, The University of Queensland

Gemberling M, Bailey TJ, Hyde DR, Poss KD (2013) The zebrafish as a model for complex tissue regeneration. Trends Genet 29:611–620. https://doi.org/10.1016/J.TIG.2013.07.003

Grasso S, Hernández JA, Chifflet S (2007) Roles of wound geometry, wound size, and extracellular matrix in the healing response of bovine corneal endothelial cells in culture. Am J Physiol Cell Physiol 293(4):C1327–C1337. https://doi.org/10.1152/ajpcell.00001.200

Green KJ, Roth-Carter Q, Niessen CM, Nichols SA (2020) Tracing the evolutionary origin of desmosomes. Curr Biol 30:R535–R543. https://doi.org/10.1016/j.cub.2020.03.047

Hay ED, Zuk A (1995) Transformations between epithelium and mesenchyme: normal, pathological, and experimentally induced. Am J Kidney Dis 26:678–690. https://doi.org/10.1016/0272-6386(95)90610-X

Jacinto A, Wood W, Balayo T, Turmaine M, Martinez-Aria A, Martin P (2000) Dynamic actin-based epithelial adhesion and cell matching during *Drosophila* dorsal closure. Curr Biol 10:1420–1426. https://doi.org/10.1016/S0960-9822(00)00796-X

Jankovics F, Brunner D (2006) Transiently reorganized microtubules are essential for zippering during dorsal closure in *Drosophila melanogaster*. Dev Cell 11:375–385. https://doi.org/10.1016/j.devcel.2006.07.014

Jones WC (1966) The structure of the porocytes in the calcareous sponge *Leucosolenia complicata* (Montagu). J R Microsc Soc 85:53–62. https://doi.org/10.1111/j.1365-2818.1966.tb02166.x

Jones WC (1957) The contractility and healing behaviour of pieces of *Leucosolenia complicata*. J Cell Sci s3–98:203–217. https://doi.org/10.1242/jcs.s3-98.42.203

Jonusaite S, Donini A, Kelly SP (2016) Occluding junctions of invertebrate epithelia. J Comp Physiol B Biochem Syst Environ Physiol 186:17–43. https://doi.org/10.1007/s00360-015-0937-1

Jopling C, Boue S, Belmonte JCI (2011) Dedifferentiation, transdifferentiation and reprogramming: three routes to regeneration. Nat Rev Mol Cell Biol 12:79–89. https://doi.org/10.1038/nrm3043

Kamran Z, Zellner K, Kyriazes H et al (2017) In vivo imaging of epithelial wound healing in the cnidarian *Clytia hemisphaerica* demonstrates early evolution of purse string and cell crawling closure mechanisms. BMC Dev Biol 17:1–15. https://doi.org/10.1186/s12861-017-0160-2

Kawamura K, Sugino Y, Sunanaga T, Fujiwara S (2008) Multipotent epithelial cells in the process of regeneration and asexual reproduction in colonial tunicates. Dev Growth Differ 50:1–11. https://doi.org/10.1111/J.1440-169X.2007.00972.X

Klarlund JK (2012) Dual modes of motility at the leading edge of migrating epithelial cell sheets. Proc Natl Acad Sci USA 109:15799–15804. https://doi.org/10.1073/pnas.1210992109

Korotkova GP (1961) Regeneration and cellular proliferation in calcareous sponge *Leucosolenia complicata* Mont. Vestnik Leningrad University 4(21):39–50

Korotkova GP (1963) Regeneration and somatic embryogenesis in calcareous sponges of the type Sycon. Vestnik Leningrad University 3:34–47

Kretschmer S, Pieper M, Klinger A, Hüttmann G, König P (2017) Imaging of wound closure of small epithelial lesions in the mouse trachea. Am J Pathol 187:2451–2460. https://doi.org/10.1016/j.ajpath.2017.07.006

Krylova D, Aleshina G, Kokryakov V, Ereskovsky A (2004) Antimicrobal properties of mesochylar granular cells of Halisarca dujardini Johnston, 1842 (Demospongiae, Halisarcida). Boll Mus Ist Biol Univ Genova 68:399–404

Kuipers D, Mehonic A, Kajita M, Peter L, Fujita Y, Duke T, Charras G, Gale JE (2014) Epithelial repair is a two-stage process driven first by dying cells and then by their neighbours. J Cell Sci 127:1229–1241. https://doi.org/10.1242/jcs.138289

Kukulies J, Naib-Majani W, Komnick H (1984) Coincident filament distribution and histochemical localization of F-actin in the enterocytes of the larval dragonfly *Aeshna cyanea*. Protoplasma 121:157–162. https://doi.org/10.1007/BF01279763

Lane NJ, Flores V (1988) Actin filaments are associated with the septate junctions of invertebrates. Tissue Cell 20:211–217. https://doi.org/10.1016/0040-8166(88)90042-0

Lanosa XA, Colombo JA (2008) Cell contact-inhibition signaling as part of wound-healing processes in brain. Neuron Glia Biol 4:27–34. https://doi.org/10.1017/S1740925X09000039

Lavrov AI, Bolshakov FV, Tokina DB, Ereskovsky AV (2018) Sewing up the wounds : the epithelial morphogenesis as a central mechanism of calcaronean sponge regeneration. J Exp Zool Part B Mol Dev Evol 330:351–371. https://doi.org/10.1002/jez.b.22830

Lavrov AI, Bolshakov FV, Tokina DB, Ereskovsky A V. (2022) Fine details of the choanocyte filter apparatus in asconoid calcareous sponges (Porifera: Calcarea) revealed by ruthenium red fixation. Zoology 150:125984. https://doi.org/10.1016/j.zool.2021.125984

Lavrov, AI, Ereskovsky AV (2022). Studying Porifera WBR Using the Calcerous Sponges Leucosolenia. In: Blanchoud, S., Galliot, B. (eds) Whole-Body Regeneration. Methods in Molecular Biology, vol 2450. Humana, New York, NY. https://doi.org/10.1007/978-1-0716-2172-1_4

Lavrov AI, Kosevich IA (2014) Sponge cell reaggregation: mechanisms and dynamics of the process. Russ J Dev Biol 45:205–223. https://doi.org/10.1134/S1062360414040067

Lavrov AI, Saidov DM, Bolshakov FV, Kosevich IA (2020) Intraspecific variability of cell reaggregation during reproduction cycle in sponges. Zoology 140. https://doi.org/10.1016/J.ZOOL.2020.125795

Ledger PW (1975) Septate junctions in the calcareous sponge *Sycon ciliatum*. Tissue Cell 7:13–18. https://doi.org/10.1016/S0040-8166(75)80004-8

Lee JSY, Gotlieb AI (2005) Microtubules regulate aortic endothelial cell actin microfilament reorganization in intact and repairing monolayers. Histol Histopathol 20:455–465

Letort G, Ennomani H, Gressin L, Théry M, Blanchoin L (2015) Dynamic reorganization of the actin cytoskeleton. F1000Research 4:1–11. https://doi.org/10.12688/f1000research.6374.1

Leys SP, Hill A (2012) The physiology and molecular biology of sponge tissues. Elsevier Ltd

Leys SP, Nichols SA, Adams EDM (2009) Epithelia and integration in sponges. Integr Comp Biol 49:167–177. https://doi.org/10.1093/icb/icp038

Leys SP, Riesgo A (2012) Epithelia, an evolutionary novelty of metazoans. J Exp Zool Part B Mol Dev Evol 318:438–447. https://doi.org/10.1002/jez.b.21442

Martin P, Lewis J (1992) Actin cables and epidermal movement in embryonic wound healing. Nature 360:179–183. https://doi.org/10.1038/360179a0

Melnikov NP, Bolshakov FV, Frolova VS et al (2022) Tissue homeostasis in sponges: Quantitative analysis of cell proliferation and apoptosis. J Exp Zool Part B Mol Dev Evol 338:360–381. https://doi.org/10.1002/jez.b.23138

Miller PW, Pokutta S, Mitchell JM, Chodaparambil JV, Clarke XDN, Nelson WJ, Weis WI, Nichols SA (2018) Analysis of a vinculin homolog in a sponge (phylum Porifera) reveals that vertebrate-like cell adhesions emerged early in animal evolution. J Biol Chem 293:11674–11686. https://doi.org/10.1074/jbc.RA117.001325

Mitchell JM, Nichols SA (2019) Diverse cell junctions with unique molecular composition in tissues of a sponge (Porifera). EvoDevo 10:1–16. https://doi.org/10.1186/s13227-019-0139-0

Nickel M, Scheer C, Hammel JU, Herzen J, Beckmann F (2011) The contractile sponge epithelium *sensu lato* – body contraction of the demosponge *Tethya wilhelma* is mediated by the pinacoderm. J Exp Biol 214:1692–1698. https://doi.org/10.1242/jeb.049148

Nier V, Deforet M, Duclos G, Yevicka HG, Cochet-Escartina O, Marcqa P, Silberzan P (2015) Tissue fusion over non-adhering surfaces. Proc Natl Acad Sci USA 112:9546–9551. https://doi.org/10.1073/pnas.1501278112

Nobes CD, Hall A (1995) Rho, Rac, and Cdc42 GTPases regulate the assembly of multimolecular focal complexes associated with actin stress fibers, lamellipodia, and filopodia. Cell 81:53–62. https://doi.org/10.1016/0092-8674(95)90370-4

Nusrat A, Delp C, Madara JL (1992) Intestinal epithelial restitution characterization of a cell culture model and mapping of cytoskeletal elements in migrating cells. J Clin Invest 89:1501–1511. https://doi.org/10.1172/JCI115741

Padua A, Klautau M (2016) Regeneration in calcareous sponges (Porifera). J Mar Biol Assoc United Kingdom 96:553–558. https://doi.org/10.1017/S0025315414002136

Pang SC, Daniels WH, Buck RC (1978) Epidermal migration during the healing of suction blisters in rat skin: a scanning and transmission electron microscopic study. Am J Anat 153:177–191. https://doi.org/10.1002/aja.1001530202

Pavans de Ceccatty M (1981) Demonstration of actin filaments in sponge cells. Cell Biol Int Rep 5:945–952. https://doi.org/10.1016/0309-1651(81)90210-1

Pavans de Ceccatty M (1986) Cytoskeletal organization and tissue patterns of epithelia in the sponge *Ephydatia mülleri*. J Morphol 189:45–65. https://doi.org/10.1002/jmor.1051890105

Pedersen KJ (1964) The cellular organization of *Convoluta convoluta*, an acoel turbellarian: a cytological, histochemical and fine structural study. Zeitschrift Für Zellforsch und Mikroskopische Anat 64:655–687. https://doi.org/10.1007/BF01258542

Peña JF, Alié A, Richter DJ, Wang L, Funayama N, Nichols SA (2016) Conserved expression of vertebrate microvillar gene homologs in choanocytes of freshwater sponges. EvoDevo 7:1–15. https://doi.org/10.1186/s13227-016-0050-x

Pope KL, Harris TJC (2008) Control of cell flattening and junctional remodelling during squamous epithelial morphogenesis in *Drosophila*. Development 135:2227–2238. https://doi.org/10.1242/dev.019802

Reffay M, Parrini MC, Cochet-Escartin O, Ladoux B, Buguin A, Coscoy S, Amblard F, Camonis J, Silberzan P (2014) Interplay of RhoA and mechanical forces in collective cell migration driven by leader cells. Nat Cell Biol 16:217–223. https://doi.org/10.1038/ncb2917

Richardson R, Metzger M, Knyphausen P, Ramezani T, Slanchev K, Kraus C, Schmelzer E, Hammerschmidt M (2016) Re-epithelialization of cutaneous wounds in adult zebrafish combines mechanisms of wound closure in embryonic and adult mammals. Development 43:2077–2088. https://doi.org/10.1242/dev.130492

Simion P, Philippe H, Baurain D, Jager M, Richter DJ, Di Franco A, Roure B, Satoh N, Queinnec E, Ereskovsky A, Lapebie P, Corre E, Delsuc F, King N, Worheide G, Manuel M (2017) A large and consistent phylogenomic dataset supports sponges as the sister group to all other animals. Curr Biol 27:958–967. https://doi.org/10.1016/j.cub.2017.02.031

Simpson TL (1984) Cell biology sponges. Springer-Verlag, New York Inc, USA

Smith CL, Varoqueaux F, Kittelmann M, Azzam RN, Cooper B, Winters CA, Eitel M, Fasshauer D, Reese TS (2014) Novel cell types, neurosecretory cells, and body plan of the early-diverging metazoan *Trichoplax adhaerens*. Curr Biol 24:1565–51572. https://doi.org/10.1016/j.cub.2014.05.046

Stramer B, Wood W, Galko MJ, Redd MJ, Jacinto A, Parkhurst SM, Martin P (2005) Live imaging of wound inflammation in *Drosophila* embryos reveals key roles for small GTPases during in vivo cell migration. J Cell Biol 168:567–573. https://doi.org/10.1083/jcb.200405120

Tamada M, Perez TD, Nelson WJ, Sheetz MP (2007) Two distinct modes of myosin assembly and dynamics during epithelial wound closure. J Cell Biol 176:27–33. https://doi.org/10.1083/jcb.200609116

Tang WJ, Watson CJ, Olmstead T, Allan CH, Kwon RY (2022) Single-cell resolution of MET- and EMT-like programs in osteoblasts during zebrafish fin regeneration. iScience 25:103784. https://doi.org/10.1016/J.ISCI.2022.103784

Ternon E, Zarate L, Chenesseau S, Croué J, Dumollard R, Suzuki MT, Thomas OP (2016) Spherulization as a process for the exudation of chemical cues by the encrusting sponge *C. crambe*. Sci Rep 6:29474. https://doi.org/10.1038/srep29474

Tétreault MP, Chailler P, Rivard N, Ménard D (2005) Differential growth factor induction and modulation of human gastric epithelial regeneration. Exp Cell Res 306:285–297. https://doi.org/10.1016/j.yexcr.2005.02.019

Thiemann M, Ruthmann A (1989) Microfilaments and microtubules in isolated fiber cells of *Trichoplax adhaerens* (Placozoa). Zoomorphology 109:89–96

Tiozzo S, Copley RR (2015) Reconsidering regeneration in metazoans: an evo-devo approach. Front Ecol Evol 3:1–12. https://doi.org/10.3389/fevo.2015.00067

Tyler S, Hooge M (2004) Comparative morphology of the body wall in flatworms (Platyhelminthes). Can J Zool 82:194–210. https://doi.org/10.1139/z03-222

Valisano L, Bavestrello G, Giovine M, Cerrano C (2006) Primmorphs formation dynamics: a screening among Mediterranean sponges. Mar Biol 149:1037–1046. https://doi.org/10.1007/s00227-006-0297-1

Vedula SRK, Hirata H, Nai MH, Brugués A, Toyama Y, Trepat X, Lim CT, Ladoux B (2014) Epithelial bridges maintain tissue integrity during collective cell migration. Nat Mater 13:87–96. https://doi.org/10.1038/nmat3814

Vedula SRK, Peyret G, Cheddadi I, Chen T, Brugues A, Hirata H, Lopez-Menendez H, Toyama Y, Neves de Almeida L, Trepat X, Lim CT, Ladoux B (2015) Mechanics of epithelial closure over non-adherent environments. Nat Commun 6:1–10. https://doi.org/10.1038/ncomms7111

Vervoort M (2011) Regeneration and development in animals. Biol Theory 6:25–35. https://doi.org/10.1007/S13752-011-0005-3

Vijayakumar S, Takito J, Hikita C, Al-Awqati Q (1999) Hensin remodels the apical cytoskeleton and induces columnarization of intercalated epithelial cells: processes that resemble terminal differentiation. J Cell Biol 144:1057–1067. https://doi.org/10.1083/jcb.144.5.1057

Wachtmann D, Stockem W, Weissenfels N (1990) Cytoskeletal organization and cell organelle transport in basal epithelial cells of the freshwater sponge *Spongilla lacustris*. Cell Tissue Res 261:145–154. https://doi.org/10.1007/BF00329447

Waterman-Storer CM, Salmon WC, Salmon ED (2000) Feedback interactions between cell-cell adherens junctions and cytoskeletal dynamics in newt lung epithelial cells. Mol Biol Cell 11:2471–2483. https://doi.org/10.1091/mbc.11.7.2471

Yin J, Lu J, Yu F-SX (2008) Role of small GTPase Rho in regulating corneal epithelial wound healing. Investig Opthalmol Vis Sci 49:900–909. https://doi.org/10.1167/iovs.07-1122

Zahm JM, Chevillard M, Puchelle E (1991) Wound repair of human surface respiratory epithelium. Am J Respir Cell Mol Biol 5:242–248. https://doi.org/10.1165/ajrcmb/5.3.242

Zahm JM, Kaplan H, Hérard AL, Doriot F, Pierrot D, Somelette P, Puchelle E (1997) Cell migration and proliferation during the in vitro wound repair of the respiratory epithelium. Cell Motil Cytoskeleton 37:33–43

Terms and Conditions

Springer Nature journal content, brought to you courtesy of Springer Nature Customer Service Center GmbH (“Springer Nature”).
Springer Nature supports a reasonable amount of sharing of research papers by authors, subscribers and authorised users (“Users”), for small-scale personal, non-commercial use provided that all copyright, trade and service marks and other proprietary notices are maintained. By accessing, sharing, receiving or otherwise using the Springer Nature journal content you agree to these terms of use (“Terms”). For these purposes, Springer Nature considers academic use (by researchers and students) to be non-commercial.
These Terms are supplementary and will apply in addition to any applicable website terms and conditions, a relevant site licence or a personal subscription. These Terms will prevail over any conflict or ambiguity with regards to the relevant terms, a site licence or a personal subscription (to the extent of the conflict or ambiguity only). For Creative Commons-licensed articles, the terms of the Creative Commons license used will apply.
We collect and use personal data to provide access to the Springer Nature journal content. We may also use these personal data internally within ResearchGate and Springer Nature and as agreed share it, in an anonymised way, for purposes of tracking, analysis and reporting. We will not otherwise disclose your personal data outside the ResearchGate or the Springer Nature group of companies unless we have your permission as detailed in the Privacy Policy.
While Users may use the Springer Nature journal content for small scale, personal non-commercial use, it is important to note that Users may not:

1. use such content for the purpose of providing other users with access on a regular or large scale basis or as a means to circumvent access control;
2. use such content where to do so would be considered a criminal or statutory offence in any jurisdiction, or gives rise to civil liability, or is otherwise unlawful;
3. falsely or misleadingly imply or suggest endorsement, approval , sponsorship, or association unless explicitly agreed to by Springer Nature in writing;
4. use bots or other automated methods to access the content or redirect messages
5. override any security feature or exclusionary protocol; or
6. share the content in order to create substitute for Springer Nature products or services or a systematic database of Springer Nature journal content.

In line with the restriction against commercial use, Springer Nature does not permit the creation of a product or service that creates revenue, royalties, rent or income from our content or its inclusion as part of a paid for service or for other commercial gain. Springer Nature journal content cannot be used for inter-library loans and librarians may not upload Springer Nature journal content on a large scale into their, or any other, institutional repository.
These terms of use are reviewed regularly and may be amended at any time. Springer Nature is not obligated to publish any information or content on this website and may remove it or features or functionality at our sole discretion, at any time with or without notice. Springer Nature may revoke this licence to you at any time and remove access to any copies of the Springer Nature journal content which have been saved.
To the fullest extent permitted by law, Springer Nature makes no warranties, representations or guarantees to Users, either express or implied with respect to the Springer nature journal content and all parties disclaim and waive any implied warranties or warranties imposed by law, including merchantability or fitness for any particular purpose.
Please note that these rights do not automatically extend to content, data or other material published by Springer Nature that may be licensed from third parties.
If you would like to use or distribute our Springer Nature journal content to a wider audience or on a regular basis or in any other manner not expressly permitted by these Terms, please contact Springer Nature at

onlineservice@springernature.com